Membrane Bound O-Acyltransferase 7 (MBOAT7) Shapes Lysosomal Lipid Homeostasis and Function to Control Alcohol-Associated Liver Injury.

Venkateshwari Varadharajan[1,3,6], Iyappan Ramachandiran[1,3,6], William J. Massey[1,3,6], Raghav Jain[9], Rakhee Banerjee[1,3,6], Anthony J. Horak 3rd[1,3,6], , Megan R. McMullen[4,6], Emily Huang[4,6], Annette Bellar[4,6], Shuhui W. Lorkowski[2], Kailash Guilshan[10], Robert N. Helsley[11], Isabella James[9], Vai Pathak[4,6], Jaividhya Dasarathy[6,7], Nicole Welch[4,6], Srinivasan Dasarathy[3,4,6], David Streem[8], Ofer Reizes[2,3], Daniela S. Allende[5,6], Jonathan D. Smith[1], Judith Simcox[9], Laura E. Nagy[3,4,6], and J. Mark Brown[1,3,6,#]

[1]Department of Cancer Biology, Lerner Research Institute of the Cleveland Clinic, Cleveland, OH, USA
[2]Department of Cardiovascular and Metabolic Sciences, Lerner Research Institute of the Cleveland Clinic, Cleveland, OH, USA
[3]Center for Microbiome and Human Health, Lerner Research Institute, Cleveland Clinic, Cleveland, OH, USA
[4]Department of Inflammation and Immunity, Lerner Research Institute, Cleveland Clinic, Cleveland, OH, USA
[5]Department of Anatomical Pathology, Cleveland Clinic, Cleveland, OH, USA
[6]Northern Ohio Alcohol Center (NOAC), Lerner Research Institute, Cleveland Clinic, Cleveland, OH, USA
[7]Department of Family Medicine, Metro Health Medical Center, Case Western Reserve University, Cleveland, OH, USA
[8]Lutheran Hospital, Cleveland Clinic, OH, USA
[9]Department of Biochemistry, University of Wisconsin-Madison, Madison, WI, USA
[10]Center for Gene Regulation in Health and Disease (GRHD), Cleveland State University, Cleveland, OH, USA
[11]Department of Pharmacology & Nutritional Sciences, Saha Cardiovascular Research Center, University of Kentucky College of Medicine, Lexington, KY, USA

[#] = To whom correspondence should be addressed: Department of Cardiovascular and Metabolic Sciences, Cleveland Clinic, Cleveland, OH 44195, USA. Tel: 216-444-8340; Fax: 216-444-9404; E-mail: brownm5@ccf.org

Running Title: Hepatocyte MBOAT7 Suppresses Alcohol-Associated Liver Disease

Key Words: hepatology, alcohol-associated liver disease, gastroenterology, metabolism

Abbreviations used: AA, arachidonic acid; ALD, alcohol-associated liver disease; ASO, antisense oligonucleotide; BMP, bis(monoacylglycerol)phosphate; Cer, ceramide; CL, cardiolipin; DAG, diacylglycerol; GWAS, genome wide association studies; LPI, lysophosphatidylinositol; LPIAT1, lysophosphatidylinositol acyltransferase 1; *MBOAT7,* membrane-bound O-acyltransferase 7; *Mboat7*^{HSKO}, *Mboat7* hepatocyte-specific knockout mice; *Mboat7*^{MSKO}, *Mboat7* myeloid-specific knockout mice; NAFLD, non-alcoholic fatty liver disease; PA, phosphatidic acid; PC, phosphatidylcholine; PE, phosphatidylethanolamine; PG, phosphatidylglycerol; PI, phosphatidylinositol; PS, phosphatidylserine; PUFA, polyunsaturated; TAG, triacylglycerol.

Abstract

Several recent genome-wide association studies (GWAS) have identified single nucleotide polymorphism (SNPs) near the gene encoding membrane-bound *O*-acyltransferase 7 (*MBOAT7*) that is associated with advanced liver diseases. In fact, a common *MBOAT7* variant (rs641738), which is associated with reduced *MBOAT7* expression, confers increased susceptibility to non-alcoholic fatty liver disease (NAFLD), alcohol-associated liver disease (ALD), and liver fibrosis in those chronically infected with hepatitis viruses B and C. The *MBOAT7* gene encodes a lysophosphatidylinositol (LPI) acyltransferase enzyme that produces the most abundant form of phosphatidylinositol 38:4 (PI 18:0/20:4). Although these recent genetic studies clearly implicate MBOAT7 function in liver disease progression, the mechanism(s) by which MBOAT7-driven LPI acylation regulates liver disease is currently unknown. Previously we showed that antisense oligonucleotide (ASO)-mediated knockdown of *Mboat7* promoted non-alcoholic fatty liver disease (NAFLD) in mice (Helsley et al., 2019). Here, we provide mechanistic insights into how *MBOAT7* loss of function promotes alcohol-associated liver disease (ALD). In

agreement with GWAS studies, we find that circulating levels of metabolic product of MBOAT7 (PI 38:4) are significantly reduced in heavy drinkers compared to age-matched healthy controls. Hepatocyte specific genetic deletion (*Mboat7*^{HSKO}), but not myeloid-specific deletion (*Mboat7*^{MSKO}), of *Mboat7* in mice results in enhanced ethanol-induced hepatic steatosis and high concentrations of plasma alanine aminotransferase (ALT). Given MBOAT7 is a lipid metabolic enzyme, we performed comprehensive lipidomic profiling of the liver and identified a striking reorganization of the hepatic lipidome upon ethanol feeding in *Mboat7*^{HSKO} mice. Specifically, we observed large increases in the levels of endosomal/lysosomal lipids including bis(monoacylglycero)phosphates (BMP) and phosphatidylglycerols (PGs) in ethanol-exposed *Mboat7*^{HSKO} mice. In parallel, ethanol-fed *Mboat7*^{HSKO} mice exhibited marked dysregulation of autophagic flux and lysosomal biogenesis when exposed to ethanol. This was associated with impaired transcription factor EB (TFEB)-mediated lysosomal biogenesis and accumulation of autophagosomes. Collectively, this works provides new molecular insights into how genetic variation in *MBOAT7* impacts ALD progression in humans and mice. This work is the first to causally link MBOAT7 loss of function in hepatocytes, but not myeloid cells, to ethanol-induced liver injury via dysregulation of lysosomal biogenesis and autophagic flux.

Introduction

End stage liver diseases account for approximately 2 million deaths annually worldwide, with nearly half of liver disease-associated deaths arising from complications of alcohol-associated and non-alcoholic fatty liver disease (NAFLD)-related cirrhosis, and the other half driven by viral hepatitis and hepatocellular carcinoma. It is generally appreciated that there are some shared mechanisms driving liver injury from viral, NAFLD, or alcohol-associated liver disease (ALD)-driven etiologies, but also etiology-specific drivers that uniquely shape the pathogenesis of liver failure. Although there has been great progress in identifying the “multiple hits” that lead to end

stage liver disease, we are only beginning to understand the cellular and molecular mechanisms driving etiology-specific liver disease progression. Within the evolving “multiple hit” theory of liver disease progression, it is clear that interactions between environmental factors (i.e. diet, microbiome, alcohol, viral infection, environmental toxins, etc.) and genetic determinants uniquely contribute to liver injury (Cohen et al., 2011; Rinella and Sanyal, 2016). Currently, the only option for end-stage liver disease is liver transplantation. However, the availability of viable donor livers is finite, and pharmacological approaches to improve outcomes are simply lacking due to our poor understanding of the underlying mechanisms of disease pathogenesis. Given this, there is a clear need to understand the genetic and environmental interactions promoting the progression of liver disease from simple steatosis to more advanced inflammatory and fibrotic disease. We address this gap here by investigating the mechanisms linking a recently identified liver disease susceptibility gene in combination with alcohol exposure.

Genome-wide association studies (GWAS) provide a powerful unbiased tool to identify new genes contributing to human disease, allowing for pinpoint accuracy in identification of new potential drug targets. This is exemplified by the recent success story of GWAS discoveries leading to rapid development of monoclonal antibodies targeting proprotein convertase subtilisin/kexin type 9 (PCSK9) for hyperlipidemia and cardiovascular diseases (Sabatine MS 2019). Since 2015, several independent GWAS studies have identified a liver disease susceptibility locus (rs641738) near the genes encoding *MBOAT7* and *TMC4* (Buch et al., 2015; Mancina et al. 2016; Vitasalo et al., 2016; Krawczyk et al., 2017; Thabet et al., 2016; Thabet et al., 2017; Teo et al., 2021). It is important to note that the rs641738 T-allele (~43% allele frequency in European ancestry populations) is associated with all major forms of liver injury including NAFLD, alcohol associated-liver disease (ALD), and viral hepatitis-induced fibrosis (Buch et al., 2015; Mancina et al. 2016; Vitasalo et al., 2016; Krawczyk et al., 2017; Thabet et

al., 2016; Thabet et al., 2017; Teo et al., 2021). The rs641738 variant is associated with a C > T missense single nucleotide polymorphism (SNP) within the first exon the *TMC4* gene, but the GTEx project shows that *TMC4* is not abundantly expressed in human liver (1.4 transcripts per million).We previously showed that mice lacking *Tmc4* (*Tmc4*$^{-/-}$) have normal high fat diet-induced hepatic steatosis (Helsley et al., 2019). We also recently demonstrated that antisense oligonucleotide (ASO)-mediated knockdown of *Mboat7* promotes insulin resistance, hepatic steatosis, hepatocyte death, inflammation, and early fibrosis in high fat diet-fed mice (Helsley et al., 2019). In parallel, four independent groups also showed that *Mboat7* loss of function promotes hepatic steatosis, inflammation, and fibrosis in mice (Meroni et al., 2020; Tanaka et al., 2021; Thangapandi et al., 2021; Xia et al., 2021). Collectively, *MBOAT7* is a genetic determinant of advanced liver disease, but how this gene shapes susceptibility to environmental cues is still an area of intense investigation.

The *MBOAT7* gene encodes a lysophospholipid acyltransferase enzyme (also known as lysophosphatidylinositol acyltransferase 1, LPIAT1), which uniquely contributes to the Land's cycle of membrane phospholipid remodeling (Shindou and Shimizu 2009). The Land's cycle is a series of phospholipase-driven deacylation and lysophospholipid acyltransferase-driven acylation reactions that shape membrane asymmetry and diversity (Shindou and Shimizu 2009). It is important to note that MBOAT7 selectively diversifies the fatty acid composition of membrane phosphatidylinositol (PI) species and not phospholipids with other head groups and exhibits acyl chain specificity for polyunsaturated fatty acids (Shindou and Shimizu, 2009; Gijón et al., 2008; Zarini et al., 2014; Caddeo A., et al., 2019; Caddeo A., et al. 2021). This substrate specificity has been observed in *in vitro* or cell-based studies (Gijón et al., 2008; Zarini et al., 2014; Caddeo A., et al., 2019; Caddeo A., et al. 2021), which has been confirmed *in vivo* in mice with diminished *Mboat7* function (Helsley et al., 2019; Meroni et al., 2020; Tanaka et al., 2021;

Thangapandi et al., 2021; Xia et al., 2021). Although MBOAT7 is well documented to directly modulate PI lipids, the Land's cycle is highly dynamic and has the potential to influence many downstream metabolic processes as well as cell signaling. Here we report that ethanol-induced perturbation of the hepatic lipidome is powerfully shaped by MBOAT7 function in hepatocytes. This MBOAT7-dependent reorganization of the hepatic lipidome in response to ethanol is also functionally tied to diminished lysosome function and defective autophagy. This work shows that MBOAT7 uniquely contributes to ethanol-induced liver injury via perturbations of hepatic lipid metabolism that extend beyond the direct remodeling of membrane PI.

Results

Heavy drinkers have reduced circulating levels of MBOAT7 enzymatic products

Given previous studies have shown that MBOAT7 is a risk locus for alcohol-associated cirrhosis (Buchs et al., 2015), we investigated whether active alcohol consumption was associated with alterations in MBOAT7 function. To address this, we measured both LPI substrates and PI products of the MBOAT7 enzymatic reaction in the circulation of healthy controls compared to confirmed heavy drinkers (**Figure 1**). Heavy drinkers were recruited and defined by an AUDIT score (Fleming et al., 1991) greater than 16, and compared to an age- and sex-matched healthy control population (**Figure 1 – figure supplement 1**). In agreement with genetic studies linking MBOAT7 variants to alcohol-associated cirrhosis (Buchs et al., 2015), we find that circulating levels of metabolic products of MBOAT7 including arachidonic acid- and eicosapentaenoic acid-containing phophosphatidylinositols (PI 38:4 & PI 38:5) are significantly reduced in heavy drinkers compared to age-matched healthy controls **(Figure 1)**. Given MBOAT7 demonstrates specificity for polyunsaturated (PUFA) acyl-CoA substrates (Gijón et al., 2008), it is important to

note that only select PUFA-containing MBOAT7 products (PI 38:4 and PI 38:5) were reduced in heavy drinkers, whereas all other molecular species of PI were unaltered. We also examined the circulating levels LPI substrates of MBOAT7 but found no significant differences between controls and heavy drinkers (**Figure 1**). These data show that excessive alcoholic intake is associated with reduced levels of MBOAT7 product lipids, which further bolsters the concept that MBOAT7 loss of function may be causally linked to ALD progression.

MBOAT7 loss of function in hepatocytes, but not myeloid cells, facilitates ethanol-induced liver injury in mice

Although there is some emerging evidence that MBOAT7 genetic variants may predispose humans to alcohol-induced liver injury (Buchs et al., 2015), not all human studies have found a significant association (Zhang et al., 2018; Stickel et al., 2018; Beaudoin et al., 2021). Importantly, a causal relationship between MBOAT7 and alcohol-induced liver injury has never been established to date. To address this, we have studied ethanol-induced liver injury in mice selectively lacking *Mboat7* in hepatocytes or myeloid cells, given the key roles that hepatocytes and myeloid cells play in the pathogenesis of ethanol-induced liver disease progression. To generate congenic hepatocyte-specific (*Mboat7*^{HSKO}) and myeloid-specific (*Mboat7*^{MSKO}) *Mboat7* knockout mice we crossed mice harboring a post-FLP recombinase conditionally targeted *Mboat7* floxed allele (Anderson et al., 2013; Massey et al., 2023) to mice transgenically expressing Cre recombinase under the albumin promoter/enhancer (Postic et al., 1999) or Cre knocked into the M lysozyme locus (Clausen et al., 1999) respectively. These independent *Mboat7*^{HSKO} and *Mboat7*^{MSKO} lines were then backcrossed mice > 10 generations into the C57BL/6J background and subsequently subjected to ethanol exposure. Compared to control mice (*Mboat7*$^{flox/flox}$), *Mboat7*^{HSKO} mice had significantly reduced *Mboat7* mRNA and protein expression in the liver (**Figure 2a,2b**), but not in other tissues (data not shown; Massey et al.,

2023). Hepatocyte-specific deletion of *Mboat7* resulted in enhanced ethanol-induced increases in liver weight and high concentrations of plasma alanine aminotransferase (ALT) (**Figure 2c,2d**). Likewise, *Mboat7*^{HSKO} mice showed elevated hepatic steatosis scores and triglyceride levels under both pair-fed and ethanol-fed conditions (**Figure 2e,2f**). However, hepatocyte-specific deletion of *Mboat7* did not significantly alter the mRNA expression for several proinflammatory cytokines/chemokines including tumor necrosis factor α (*Tnfα*), transforming growth factor β (*Tgfβ*), monocyte chemoattractant protein 1 (*Mcp1*), or interleukins 1β (*IL-1β*) or 6 (*IL-6*) in either pair-fed or ethanol-fed conditions (**Figure 2g**). These data demonstrate that MBOAT7 function in hepatocytes is a critical determinant of ethanol-induced liver injury, but we also wanted to explore a potential role for MBOAT7 in non-parenchymal cells given the key roles that macrophages and neutrophils play in ALD.

It is important to note during the preparation of this manuscript, an independent study discovered a potential role for MBOAT7 in suppressing toll-like receptor (TLR) signaling and pro-inflammatory cytokine production in macrophages and Kupffer cells in the context of non-alcoholic fatty liver disease (NAFLD) (Alharthi et al., 2022). Furthermore, early studies examining the expression and substrate specificity for diverse lysophospholipid acyltransferases showed that MBOAT7-driven PI remodeling was highly active in human neutrophils where it can modulate the production of pro-inflammatory arachidonic acid-derived lipid mediators (Gijón et al., 2008). Therefore, we generated myeloid-specific (*Mboat7*^{MSKO}) *Mboat7* knockout mice to further interrogate cell autonomous roles in ALD progression. First to confirm efficient deletion in myeloid cells, we isolated both bone marrow-derived and thioglycolate-elicited macrophages from control and myeloid-specific (*Mboat7*^{MSKO}) *Mboat7* knockout mice, which confirmed essentially no detectable MBOAT7 protein in *Mboat7*^{MSKO} mice (**Figure 2 – figure supplement 1**). In contrast to the enhanced ethanol-induced liver injury seen in *Mboat7*^{HSKO} mice (**Figure 2**), myeloid-specific (*Mboat7*^{MSKO}) *Mboat7* deletion resulted in unaltered ethanol-induced effects on

body weight, liver weight, circulating levels of aspartate and alanine aminotransferases (AST and ALT), liver triglyceride, and cytokine expression (**Figure 2 – figure supplement 1**). Collectively, these results demonstrate that MBOAT7 loss of function in hepatocytes, but not myeloid cells, facilitates ethanol-induced liver injury in mice.

Ethanol exposure reorganizes the hepatic lipidome in a MBOAT7-dependent manner

Given the fact that ethanol exposure is well known to reorganize hepatic lipid metabolism, we performed comprehensive lipidomic profiling of the liver to understand how MBOAT7 could potentially shape ethanol-induced lipid metabolism in the liver. First, we used a targeted approach to measure the levels of MBOAT7 substrate LPIs and product PIs. Compared to control mice (*Mboat7*$^{flox/flox}$), *Mboat7*^{HSKO} mice had significant accumulation of palmitate- and oleate-containing LPI substrate lipids (LPI 16:0 and LPI 18:1), with large accumulation of LPI 16:0 under ethanol-fed conditions (**Figure 3a**). When we examined PI species, we confirmed previous findings that *Mboat7*^{HSKO} mice have reduced levels of the major arachidonic acid-containing PI (PI 38:4) and also striking reductions in PI 38:3 under both pair- and ethanol-fed conditions (**Figure 3b**). In addition, *Mboat7*^{HSKO} mice also have accumulation of several other PI species including PI 34:1, PI 36:1, PI 36:2, PI 38:6, and PI 40:6, some of which are exacerbated in the ethanol-fed group (**Figure 3c**). Although many of these changes in MBOAT7's substrate LPIs and product PIs are expected based on MBOAT7's substrate specificity and previous literature, there is a clear interaction between ethanol and MBOAT7 uncovered here that has not been observed in studies using NAFLD-related models (Tanaka et al., 2021; Thangapandi et al., 2021; Xia et al., 2021).

Given this unexpected interaction between ethanol exposure and MBOAT7 within the inositol-containing phospholipid pool, we examined the hepatic lipidome more broadly. Using untargeted lipidomics, we identified a striking remodeling of the global hepatic lipidome upon ethanol feeding

in *Mboat7*^{HSKO} mice (**Figure 3 & Figure 3 – figure supplements 1-11**). Unexpectedly, we observed a large increase in the levels of endosomal/lysosomal lipids including bis(monoacylglycero)phosphates (BMPs) and their outer mitochondrial membrane precursor phosphatidylglycerols (PGs) in ethanol-exposed *Mboat7*^{HSKO} mice (**Figure 3e-3g; Figure 3 – figure supplement 3 & 4**). In addition, *Mboat7*^{HSKO} mice had elevated levels of cardiolipin species, which are known to localize to mitochondria (**Figure 3e,3h; Figure 3 – figure supplement 5**). Under the pair- and ethanol-fed conditions studies here, *Mboat7*^{HSKO} mice also exhibited some more minor alterations in certain species of phosphatidylcholine (PC), phosphatidylethanolamine (PE), phosphatidylserine (PS), sphingomyelin (SM), ceramides (Cer), diacylglycerols (DAG), and ether-linked phospholipids (**Figure 3e; Figure 3 – figure supplements 1,2,6-11**). Although several recent studies examining hepatocyte-specific *Mboat7*^{HSKO} mice have found more limited effects on the global lipidome under experimental conditions designed to stimulate non-alcoholic steatohepatitis (NASH) (Tanaka et al., 2021; Thangapandi et al., 2021; Xia et al., 2021), here we show that upon ethanol exposure, hepatocyte MBOAT7 plays a major role in shaping endosomal/lysosomal lipid homeostasis.

Mboat7^{HSKO} mice have dysregulated lysosomal function in response to ethanol

Given the accumulation of endosomal/lysosomal lipids including BMPs seen in ethanol-fed *Mboat7*^{HSKO} mice, we hypothesized that ethanol may perturb lysosome function in a MBOAT7-driven manner to promote liver injury. It is well known that BMPs commonly accumulate in both drug-induced and genetic lysosomal storage disorders (Gruenberg 2020; Showalter et al., 2020; Hullin-Matsuda et al., 2014), and due to their cone-shaped structure BMPs can contribute to significant membrane asymmetry that impacts intracellular lipid sorting, apoptosis, and autophagic flux (Gruenberg 2020; Showalter et al., 2020; Hullin-Matsuda et al., 2014). At the same time, there is emerging evidence that chronic ethanol exposure can reduce the expression

of transcription factor EB (TFEB), which is a master regulator of lysosomal biogenesis and autophagy-associated gene expression (Chao et al., 2018). Given the role that lysosomal dysfunction plays in ethanol-induced liver injury (Chao et al., 2018; Bala and Szabo 2018), and the unexpected accumulation of BMP lipids in *Mboat7*^{HSKO} mice, we next investigated TFEB-mediated lysosomal biogenesis and autophagy regulation in *Mboat7*^{HSKO} mice challenged with ethanol (**Figure 4**). First, *Mboat7*^{HSKO} mice showed elevated levels of key autophagy regulatory proteins LC3-I/II and p62 in the liver, particularly under ethanol-fed conditions (**Figure 4a**). Interestingly, *Mboat7*^{HSKO} mice also had increased total levels of the mammalian target of rapamycin (mTOR) (**Figure 4a**), which is a well-known master regulator of autophagic flux. The accumulation of p62 and LC3-I/II cannot distinguish between enhanced or defective autophagic flux, so we next examined potential alterations in lysosome abundance and function. Interestingly, both mRNA and protein levels of lysosomal marker proteins LAMP-1 and LAMP-2 were reduced in ethanol-fed *Mboat7*^{HSKO} mice (**Figure 4a,4d**). Furthermore, compared to control mice fed ethanol, we found that ethanol *Mboat7*^{HSKO} mice had generally reduced expressions levels of TFEB target genes and proteins associated with lysosome acidification and lipid turnover including ATPase H+ transporting V1 subunits A,H, and D (*Atp6v1a, Atp6v1h, Atp6v1d*), α galactosidase A (*Gla*), chloride channel 7 α (*Clcn7*), and mucolipin TRP cation channel 1 (*Mcoln1*) (**Figure 4a,4d**). Similarly, the mRNA expression, and total and nuclear protein abundance of TFEB was reduced in ethanol-fed *Mboat7*^{HSKO} mice compared to ethanol-fed *Mboat7*$^{flox/flox}$ control mice (**Figure 4a,4b,4d**). In contrast, the expression of key autophagy related genes including *Atg2b, Atg3, Atg7, Atg8/LC3*, and Unc-51-like autophagy activating kinase 1 (*Ulk1*) were significantly elevated in ethanol-fed *Mboat7*^{HSKO} mice compared to ethanol-fed *Mboat7*$^{flox/flox}$ control mice (**Figure 4d**).

We next investigated the cell autonomous effects of ethanol on wild type human Huh7 hepatoma cells or Huh7 cells genetically lacking *MBOAT7* (*MBOAT7Δ*-Huh7). In agreement with

what we found in mouse liver, *MBOAT7Δ*-Huh7 cells had reduced levels of total TFEB and lysosomal marker proteins including LAMP1-, LAMP-2, and ATP6V1A, (**Figure 4 – figure supplement 1**). Furthermore, *MBOAT7*Δ-Huh7 cells had increased levels of LC3 and total mTOR, which was particularly apparent upon ethanol exposure (**Figure 4 – figure supplement 1**). We next assessed lysosome protein degradation activity in wild type and MBOAT7Δ-Huh7 hepatoma cells by measuring the degradation of an exogenous lysosome indicator, quantified via median Bodipy/Alexa647 fluorescence ratio. In the absence of ethanol treatment, there was no significant difference in the lysosomal activity between wild type and MBOAT7Δ-Huh7 cells. Lysosome activity was increased by 42% in wild type cells with ethanol treatment vs. no treatment ($p<0.001$. **Figure 4c**), in agreement with increased mRNA levels of several lysosomal hydrolases (**Figure 4d**). However, the lysosome activity was decreased by 45% in MBOAT7Δ-Huh7 vs. wild type cells treated with ethanol ($p<0.001$, **Figure 4c**). Collectively, in the presence of EtOH, deletion of *MBOAT7* in mouse or human hepatocytes results in defective TFEB-mediated lysosomal biogenesis and lysosome activity, which would be expected to lead to impaired autophagic flux.

Discussion

This manuscript builds on our initial observation that ASO-mediated knockdown of *Mboat7* promotes NAFLD progression, hyperinsulinemia, and insulin resistance in mice (Helsley et al., 2019). Here we have further clarified the cell autonomous roles of *Mboat7* in ethanol-driven liver injury by comparing metabolic phenotypes in hepatocyte-specific (*Mboat7*^{HSKO}) and myeloid-specific (*Mboat7*^{MSKO}) mice. The major findings of the current study include the following: (1) MBOAT7 product PI species (PI 38:4 and PI 38:5) are reduced in the circulation of human consuming high levels of alcohol, (2) MBOAT7 loss of function in hepatocytes, but not myeloid cells, promotes ethanol-induced liver injury in mice, (3) Hepatocyte-specific deletion of *Mboat7*

results in expected alterations in substrate LPI and product PI lipids, but unexpectedly alters lysosomal/endosome BMP lipids in an ethanol-driven manner, (4) Genetic deletion in mouse or human hepatocytes results in dysregulation of lysosomal biogenesis and autophagic flux, particularly under ethanol-challenged conditions. This works provides new insights into how genetic variation in *MBOAT7* may impact ALD progression in humans and mice. Importantly, this work is the first to causally link MBOAT7 loss of function in hepatocytes, but not myeloid cells, to ethanol-induced liver injury via dysregulation of lysosomal biogenesis and autophagic flux. Although not all human studies agree there is a uniform association between the rs641738 SNP with alcohol-associated liver disease, our work indicate a very powerful interaction between MBOAT7 loss of function and ethanol-induced liver injury.

Here we have identified a striking reorganization of the hepatic lipidome in *Mboat7*^{HSKO} mice when exposed to ethanol (**Figure 3; Figure 3 – figure supplements 1-11**). In previous independent studies examining lipid alterations in *Mboat7*^{HSKO} mice under experimental conditions to elicit NAFLD and fibrosis (i.e. high fat diets or methionine/choline-deficient diets), the global lipidomic alterations in the liver were much more confined to inositol-containing phospholipids and triacylglycerols (Tanaka et al., 2019; Thangapandi et al., 2019). It is important to note that the work of Xia and colleagues did previously report increased levels on PG lipids specifically in isolated endoplasmic reticulum (ER) membranes from *Mboat7*^{HSKO} mice, but our work confirms and extends this to show that not only PG but precursor BMPs are significantly elevated in *Mboat7*^{HSKO} mice, particularly when challenged with ethanol. It is still unclear how MBOAT7 impacts endosomal/lysosomal BMP and mitochondrial lipids such as PG and CL under ethanol-exposed conditions, but our work clearly indicates that ethanol reorganizes the global liver lipidome in a MBOAT7-dependent manner. It is most likely that the accumulation of BMP and PG lipids seen in ethanol-challenged *Mboat7*^{HSKO} mice are not directly related to the lysophospholipid acyltransferase activity of MBOAT7. Instead, it is more plausible that the

accumulation of BMPs and PGs seen in *Mboat7*^{HSKO} mice is secondary to indirect reorganization of the arachidonate PI cycle or other related lipid metabolic pathways coordinated at the ER.

For instance, the arachidonate PI cycle is initiated in the ER where inositol is added to CDP-diacylglycerol (18:0/20:4) by phosphatidylinositol synthase (PIS) to produce the exact same metabolic product of MBOAT7 (PI 38:4). It is likely that both PIS-generated as well as MBOAT7-generated PI 38:4 can serve as a substrate for phosphatidylinositol kinases to form the key second messengers known as PI phosphates [PIPs including PI(18:0/20:4)-4P, PI(18:0/20:4)-4,5P_2,] and related lipid mediators downstream of phospholipase C in the arachidonate PI cycle [IP3, DAG(18:0/20:4), PA(18:0/20:4), and CDP-DAG(18:0/20:4). It is important to note that seminal work by Anderson and colleagues (Anderson et al., 2013) found that total PIPs, PI(18:0/20:4)-4P, and PI(18:0/20:4)-4,5P_2 were significantly reduced in global *Mboat7*$^{-/-}$ mice. In fact, more than 85% of PIP species in cultured cells have an *sn*-1 18:0 and *sn*-2 20:4 acyl chain composition (i.e., in part originate from the MBOAT7 and PIS product PI 38:4) (Clark et al., 2011; Rouzer et al., 2007). These reductions in PIPs seen with *Mboat7* deficiency (Anderson et al., 2013) could have important consequences in cellular signal transduction, given that PIPs are common second messengers generated downstream of ligand activation of numerous receptor systems including hormone, growth factor, cytokine, and chemokine receptors (Wymann and Schneiter 2008; Pemberton et al., 2020; Fruman et al., 2017; Hoxhaj and Manning 2020). PIPs also play diverse roles in shaping protein-lipid interactions, membrane fusion events, vesicular transport, solute channel function, and cytoskeletal arrangement (Wymann and Schneiter 2008; Pemberton et al., 2020; Fruman et al., 2017; Hoxhaj and Manning 2020). Most relevant to this work, anionic lipids play very important roles in controlling membrane dynamics that shape nearly all steps of autophagy including initiation of autophagosome biogenesis and autophagosome-lysosome fusion (Baba and Balla 2020; Schink et al., 2016). Collectively, given the fact that MBOAT7 generates the most abundant species of PI (PI 38:4), and key cellular

PIPs [PI(18:0/20:4)-4P, and PI(18:0/20:4)-4,5P_2] there is a strong potential that the primary alterations in PI and PIP lipids could broadly alter cellular signal transduction, endosomal/lysosomal lipid sorting, membrane fusion events, vesicular transport, solute channel function, cytoskeletal arrangement, and autophagic flux.

Collectively, this works provides new cellular and molecular insights into how genetic variation in *MBOAT7* impacts ALD progression in humans and mice. This work is the first to causally link MBOAT7 loss of function in hepatocytes, but not myeloid cells, to ethanol-induced liver injury via dysregulation of lysosomal biogenesis and autophagic flux and broaden our understanding of the lipid metabolic mechanisms promoting ethanol-induced liver injury. This work also shows that MBOAT7-driven LPI acylation in the ER can indirectly impact both lysosomal (BMP) and mitochondrial (CL and PG) lipids which can have broad impacts on autophagy described here, as well as defective fatty acid oxidation as we originally reported in high fat diet-fed mice (Helsley et al., 2019). The results of this work have broad potential implications in the management of both alcoholic- and non-alcoholic fatty liver disease, indicating that strategies that effectively restore both lysosomal and mitochondrial function may hold some therapeutic promise in humans with the common MBOAT7 rs641738 variant.

KEY RESOURCE TABLE:

Key Resource Table					
Reagent type (species) or resource	Designation	Source or Reference	Identifiers	Additional Information	Research Resource Identifiers (RRID)
Genetic reagent (*M.musculus*)	*Mboat7tm1a(KOMP)Wtsi/ Mboat7tm1a(KOMP)Wtsi*	PMID: 23472195			RRID:MGI:5510874
Genetic reagent (*M.musculus*)	*B6N.Cg-Speer6-ps1$^{Tg(Alb-cre)21Mgn}$/J*	Jackson Laboratory	Stock#: 018961		RRID:IMSR_JAX:018961
Genetic reagent (*M.musculus*)	*B6.129P2-Lyz2$^{tm1(cre)Ifo}$/J*	Jackson Laboratory	Stock#: 004781		RRID:IMSR_JAX:004781
Antibody	Anti-MBOAT7 (Rat monoclonal)	PMID: 23097495		1:1000	RRID: AB_2813851
Antibody	Anti-Rat-HRP	Cell Signaling	Cat#: 7077	1:5000	RRID: AB_10694715
Antibody	LC3A/B (D3U4C) XP® Rabbit mAb	Cell Signaling	Cat#: 12741	1:1000	RRID: AB_2617131
Antibody	SQSTM1/p62 Antibody	Cell Signaling	Cat#: 5114	1:1000	RRID: AB_10624872
Antibody	mTOR (7C10) Rabbit mAb	Cell Signaling	Cat#: 2983	1:1000	RRID: AB_2105622
Antibody	TFEB Rabbit mAb 37785	Cell Signaling	Cat#: D207D	1:1000	
Antibody	LAMP1 (D2D11) XP® Rabbit mAb	Cell Signaling	Cat#: 9091	1:1000	
Antibody	LAMP2 (D5C2P) Rabbit mAb #49067	Cell Signaling	Cat#: 49067	1:1000	RRID: AB_2799349
Antibody	ATP6V1A polyclonal antibody	GeneTex	Cat#: GTX110815	1:1000	
Antibody	Anti-GAPDH-HRP (Rabbit monoclonal)	Cell Signaling	Cat#: 8884	1:5000	RRID: AB_11129865
Antibody	Lamin A/C (4C11) Mouse mAb	Cell Signaling	Cat#: 4777	1:1000	RRID:
Antibody	HRP-conjugated Beta Actin Monoclonal antibody	Proteintech	Cat#: HRP-60008	1:10000	RRID: AB_2289225
Commercial assay kit	ALT kit	Sekisui Diagnostics	318-30		
Commercial assay kit	AST kit	Sekisui Diagnostics	319-30		
Commercial assay kit	Liver TG	Wako	994-02891		
Commercial assay kit	Microsome Isolation	Abcam	ab206995		
Commercial assay kit	NE-PER™ Nuclear and Cytoplasmic Extraction Reagents	ThermoFisher Scientific	78833		
Commercial assay kit	Supersignal West Pico Plus substrate	ThermoFisher Scientific	34577		
Chemical or Solvent	Ammonium formate	Honeywell	Cat# 55674		
Chemical or Solvent	Methanol	Honeywell	Cat# LC230-4		
Chemical or Solvent	Water	Honeywell	Cat# LC365-4		
Chemical or Solvent	Acetonitrile	Honeywell	Cat# LC015-4		
Chemical or Solvent	Isopropanol	Fisher Scientific	Cat# A461-4		

Chemical or Solvent	Ethyl acetate	Sigma-Aldrich	Cat# 650528		
Chemical or Solvent	Formic acid	Thermo Scientific	Cat# 28905		
Chemical Compound	FA 18:0$_{d35}$	Cayman Chemical	Cat# 9003318		
Chemical Compound	ACar 18:1$_{d3}$	Cayman Chemical	Cat# 26578		
Chemical Compound	BMP 14:0_14:0	Avanti	Cat# 857131		
Chemical Compound	PG 15:0_18:1$_{d7}$	Avanti	Cat# 91640		
Chemical Compound	Cer d18:1$_{d7}$_15:0	Avanti	Cat# 860681P		
Chemical Compound	PA 15:0_18:1$_{d7}$	Avanti	Cat# 791642		
Chemical Compound	SPLASH LipidoMix II	Avanti	Cat# 330709		
Chemical Compound	BMP 18:1_18:1	Avanti	Cat# 857133P		
Chemical Compound	PG 18:1_18:1	Avanti	Cat# 840475P		
Sequence Based Reagent	Mboat7 Fwd	Sigma	5'-CATGCGGTACTGGAACATGA-3'		
Sequence Based Reagent	Mboat7 Rev	Sigma	5'-CCAGTAGGCGCTCAGCAG-3'		
Sequence Based Reagent	Cyclophilin A Fwd	Sigma	5'-GCGGCAGGTCCATCTACG-3'		
Sequence Based Reagent	Cyclophilin A Rev	Sigma	5'-GCCATCCAGCCATTCAGTC-3'		
Sequence Based Reagent	Tnfalpha Fwd	Sigma	5'-CCACCACGCTCTTCTGTCTAC -3'		
Sequence Based Reagent	Tnfalpha Rev	Sigma	5'-AGGGTCTGGGCCATAGAACT-3'		
Sequence Based Reagent	IL-1β Fwd	Sigma	5'-AGTTGACGGACCCCAAAAG -3'		
Sequence Based Reagent	IL-1β Rev	Sigma	5'-AGCTGGATGCTCTCATCAGG -3'		
Sequence Based Reagent	Tgf β Fwd	Sigma	5'-TGGAGCAACATGTGGAACTC-3'		
Sequence Based Reagent	Tgf βRev	Sigma	5'-CAGCAGCCGGTTACCAAG-3'		
Sequence Based Reagent	IL-6 Fwd	Sigma	5'-GCTACCAAACTGGATATAATCAGGA-3'		
Sequence Based Reagent	IL-6 Rev	Sigma	5'-CCAGGTAGCTATGGTACTCCAGAA-3'		
Sequence Based Reagent	Mcp-1 Fwd	Sigma	5'-TTCCTCCACCACCATGCAG-3'		

Sequence Based Reagent	Mcp-1 Rev	Sigma	5'-CCAGCCGGCAACTGTGA-3'		
Sequence Based Reagent	TFEB Fwd	Sigma	5'-CCAGAAGCGAGAGCTCACAGAT-3'		
Sequence Based Reagent	TFEB Rev	Sigma	5'-TGTGATTGTCTTTCTTCTGCCG-3'		
Sequence Based Reagent	Lamp-1 Fwd	Sigma	5'-AGCATACCGGTGTGTCAGTG-3'		
Sequence Based Reagent	Lamp-1 Rev	Sigma	5'-GTTGGGGAAGGTCCATCCTG-3'		
Sequence Based Reagent	Lamp-2 Fwd	Sigma	5'-TGCAGTGCAGATGAAGACAAC-3'		
Sequence Based Reagent	Lamp-2 Rev	Sigma	5'-GCTATGGGCACAAGGAAGTTG-3'		
Sequence Based Reagent	Ctsa Fwd	Sigma	5'-GCTACCTCAGAGCATCGGAC-3'		
Sequence Based Reagent	Ctsa Rev	Sigma	5'-GTTAAGCCAAAGCACCACGG-3'		
Sequence Based Reagent	Gba Fwd	Sigma	5'-GCCTCCCAGAAGAAGACACC-3'		
Sequence Based Reagent	Gba Rev	Sigma	5'-ATATCCCCTGGCTGACCCTT-3'		
Sequence Based Reagent	Gla Fwd	Sigma	5'-TTGGGGTCAGAGCA TTGGAC-3'		
Sequence Based Reagent	Gla Rev	Sigma	5'-AGTCATAACCTGCATCCCGC-3'		
Sequence Based Reagent	Psap Fwd	Sigma	5'-CAGCAGATGGTCTGGAGCAA-3'		
Sequence Based Reagent	Psap Rev	Sigma	5'-CAAGTTCCCAGCTTCGGTGA-3'		
Sequence Based Reagent	Clcn7 Fwd	Sigma	5'-CGAGATGCCTATCCACGCTT-3'		
Sequence Based Reagent	Clcn7 Rev	Sigma	5'-CCCGGAAGAGCTTGAACACT-3'		
Sequence Based Reagent	Mcoln1 Fwd	Sigma	5'-TGGGCCAATGGATCAGCTTT-3'		

Sequence Based Reagent	Mcoln1 Rev	Sigma	5'-GTTCTTGTAACTGGCGCTGC-3'		
Sequence Based Reagent	Atp6v1h Fwd	Sigma	5'-AAGACCAGCAGGTTCGCTAC-3'		
Sequence Based Reagent	Atp6v1h Rev	Sigma	5'-TGCAGAAAGGCTGAACAGGT-3'		
Sequence Based Reagent	Atp6v1d Fwd	Sigma	5'-GAGCACAGACTGGTCGAAA-3'		
Sequence Based Reagent	Atp6v1d Rev	Sigma	5'-AGCTGTCAGTTCCTTCGTGG-3'		
Sequence Based Reagent	ULK1 Fwd	Sigma	5'-ACCATTGTCTACCAGTGT-3'		
Sequence Based Reagent	ULK1 Rev	Sigma	5'-AGTGTCTTGTTCTTCTCATAA-3'		
Sequence Based Reagent	Atg2b Fwd	Sigma	5'-CCTCCACTCTCAGAATCA-3'		
Sequence Based Reagent	Atg2b Rev	Sigma	5'-GTCCATCACACGAACATAA-3'		
Sequence Based Reagent	Atg3 Fwd	Sigma	5'-TCACAACACAGGTATTACAG-3'		
Sequence Based Reagent	Atg3 Rev	Sigma	5'-CTTCCTCGTCTTCTTCATC-3'		
Sequence Based Reagent	Atg7 Fwd	Sigma	5'-CAGAAGAAGTTGAACGAGTA-3'		
Sequence Based Reagent	Atg7 Rev	Sigma	5'-CAGAGTCACCATTGTAGTAAT-3'		
Sequence Based Reagent	Lc3 Fwd	Sigma	5'-GCTCTTTGTTGGTGTGTA-3'		
Sequence Based Reagent	Lc3 Rev	Sigma	5'-TCTTCTGTTGCTGTTGTC-3'		

METHODS

Human studies

Healthy Control and Heavy Drinking Patient Selection - Healthy controls or heavy drinkers with an AUDIT score greater than >16 were recruited from the Clinical Research Unit at the Cleveland Clinic or MetroHealth Hospital in Cleveland, Ohio based on medical history and physical examination. The study protocol was approved by the Institutional review board for the Protection of Human Subjects in Research at the Cleveland Clinic (IRB 17-718) and MetroHealth Hospital Cleveland (IRB 18-00911). All methods were performed in accordance with the internal review board's guidelines and regulations, and written, informed consent was obtained from all subjects. Subject demographics are shown in Figure 1 – figure supplement 1.

Mice and experimental diets

To generate conditional *Mboat7* knockout mice, we obtained "knockout first" (Mboat7$^{tm1a(KOMP)Wtsi}$) mice from Dr. Philip Hawkins (Anderson et al., 2013), and crossed these mice with mice transgenically expressing FLP recombinase to remove the NEO cassette resulting in a conditional *Mboat7* floxed allele. The FLP transgene was then subsequently bred out of the line and resulting *Mboat7*$^{flox/WT}$ mice, which were used to expand further downstream tissue-specific knockout lines. To generate congenic hepatocyte-specific (*Mboat7*^{HSKO}) and myeloid-specific (*Mboat7*^{MSKO}) *Mboat7* knockout mice we crossed mice harboring a post-FLP recombinase conditionally-targeted *Mboat7* floxed allele (Anderson et al., 2013; Massey et al., 2023) to mice transgenically expressing Cre recombinase under the albumin promoter/enhancer (Postic et al., 1999) or Cre knocked into the M lysozyme locus (Clausen et al., 1999) respectively. These independent *Mboat7*^{HSKO} and *Mboat7*^{MSKO} lines were then backcrossed mice > 10 generations into the C57BL/6J background and subsequently subjected to ethanol exposure. Confirmation of sufficient backcrossing into the C57BL/6J background was confirmed by mouse

genome single nucleotide polymorphism (SNP) scanning at the Jackson Laboratory (Bar Harbor, ME). Age- and weight-matched female (8-10 weeks old) control (Mboat7$^{flox/flox}$), hepatocyte-specific *Mboat7* knockout mice (Mboat7^{HSKO}), or myeloid-specific *Mboat7* knockout mice (Mboat7^{MSKO}) were maintained on a chow diet and randomized into pair- and ethanol-fed groups using the NIAAA model (Bertola et al., 2013). Briefly, mice were initially fed with control Lieber-DeCarli diet ad libitum for 5 days to acclimatize them to liquid diet. Afterward, ethanol (EtOH)-fed groups were allowed free access to the ethanol Lieber-DeCarli diet containing 5% (vol/vol) ethanol for 10 days, and control groups were pair-fed with the isocaloric substituted maltose dextrins as control diet. At day 11, ethanol-fed and pair-fed mice were gavaged in the early morning with a single dose of ethanol (5 g/kg body weight) or isocaloric maltose dextrin, respectively, and euthanized 6 hours later. (Bertola et al., 2013). All mice were maintained in an Association for the Assessment and Accreditation of Laboratory Animal Care, International-approved animal facility, and all experimental protocols were approved by the Institutional Animal Care and Use Committee of the Cleveland Clinic (IACUC protocols # 2018-2053 and # 00002499).

Histological analysis and imaging

Hematoxylin and eosin (H&E) staining of paraffin-embedded liver sections was performed as previously described (Gromovsky et al., 2017; Warrier et al., 2015; Brown et al., 2010; Brown et al., 2008a; Brown et al. 2008b). Histopathologic evaluation was scored in a blinded fashion by a board-certified pathologist with expertise in gastrointestinal/liver pathology (Daniela S. Allende – Cleveland Clinic). H&E slides were scanned using a Leica Aperio AT2 Slide Scanner (Leica Microsystems, GmbH, Wetzlar, Germany) and images were processed using ImageScope (Aperio, Software Version 12.1)

Immunoblotting

Whole tissue homogenates were made from tissues in a modified RIPA buffer as previously described (Warrier et al., 2015; Helsley et al., 2019; Schugar et al., 2017; Lord et al., 2016), and protein was quantified using the bicinchoninic assay (Pierce). Proteins were separated by 4–12% SDS-PAGE, transferred to polyvinylidene difluoride membranes, and then proteins were detected after incubation with specific antibodies as previously described (Warrier et al., 2015; Helsley et al., 2019; Schugar et al., 2017; Lord et al., 2016) and listed in the Key resources table.

Real-time PCR analysis of gene expression

Tissue RNA extraction and qPCR analysis was performed as previously described (Helsley et al., 2019). The mRNA expression levels were calculated based on the ΔΔ-CT method using cyclophilin A as the housekeeping gene. qPCR was conducted using the Applied Biosystems 7500 Real-Time PCRsystem. All primer sequences are listed in the Key resources table.

Plasma and liver biochemistries

To determine the level of hepatic injury in mice fed HFD, plasma was used to analyze alanine aminotransferase (ALT) levels using enzymatic assays as previously described (Helsley et al., 2019). Extraction of liver lipids and quantification of total plasma and hepatic triglycerides was conducted using enzymatic assays as described previously (Helsley et al., 2019; Gromovsky et al., 2017).

Liver lipid extraction

Lipids were extracted from liver samples as previously described (Jain et al., 2022). Samples were kept on ice throughout the extraction. Briefly, liver was homogenized in 500uL of 3:1:6 isopropanol:water:ethyl acetate containing internal standard in ceramic bead tubes (Qiagen

#13113-50) using the TissueLyzer II (Qiagen #9244420). Samples were centrifuged at 16,000xg for 10min at 4°C and the lipid containing supernatant was transferred to a new 1.5mL tube. Lipid extracts were dried in a SpeedVac (Thermo Savant RVT5105) and resuspended in 150uL of methanol. Samples were kept at 4°C for no more than one week before analysis.

Targeted quantification of lysophosphatidylinositol (LPI) and phosphatidylinositol (PI) lipids

Quantitation of LPI and PI species was performed as previously described (Helsley et al., 2019) Briefly, LPI and PI standards (LPI 16:0, LPI 18:0, LPI 18:1, LPI 20:4, PI 38:4) and the two internal standards (LPI 17:1-d31, PI 34:1-d31) were purchased Avanti Polar Lipids. HPLC grade water, methanol and acetonitrile were purchased from Thermo Fisher Scientific. Standard LPI and PI species at concentrations of 0, 5, 20, 100, 500 and 2000 ng/ml were prepared in 90% methanol containing 2 internal standards at the concentration of 500 ng/ml. Samples were injected into the Shimadzu LCMS-8050 for generating the internal standard calibration curves. A triple quadrupole mass spectrometer (Quantiva, Thermos Fisher Scientific, Waltham, MA, USA) was used for analysis of LPI and PI species. The mass spectrometer was coupled to the outlet of an UHPLC system (Vanquish, Thermos Fisher Scientific, Waltham, MA, USA), including an auto sampler with refrigerated sample compartment and inline vacuum degasser. The HPLC eluent was directly injected into the triple quadrupole mass spectrometer and the analytes were ionized at ESI negative mode. Analytes were quantified using Selected Reaction Monitoring (SRM) and the SRM transitions (m/z) were 571 → 255 for LPI 16:0, 599 → 283 for LPI 18:0, 597 → 281 for LPI 18:1, 619 → 303 for LPI 20:4, 885 → 241 for PI 38:4, 583 → 267 for internal standard LPI 17:1, and 866 → 281 for internal standard PI 34:1-d31. Xcalibur software was used to get the peak area for both the internal standards and LPI and PI species. The internal standard calibration curves were used to calculate the concentration of LPI and PI species in the samples.

Untargeted Lipidomics

Untargeted lipidomics was performed using an Agilent 1290 Infinity II liquid chromatograph equipped with a Waters Acquity BEH C18 column (1.7 µm 2.1 × 100 mm) coupled to an Agilent 6546 Q-TOF mass spectrometer. Mobile phase A was 60:40 acetonitrile:water and B was 90:9:1 isopropanol:acetonitrile:water with both phases buffered with 10mM ammonium formate and 0.1% formic acid. The gradient was as follows: starting at 15% B to 30% B at 2.40 min, 48% at 3 min, 82% at 13.2 min, 99% at 13.8 min then held at 99% until 15.4 min before equilibrating 15%, held until 20 min. Samples were analyzed in both positive and negative ionization in separate experiments with the following MS parameters: drying gas flowing 12 L/min at 250°C, nebulizer at 30 psi and sheath gas flowing 11 L/min at 300°C for positive mode. The sheath gas flow was 12 L/min at 375°C with a nebulizer pressure of 30 psi in negative mode. Both ionizations had the same voltage for capillary (4000 V), skimmer (75 V), fragmentor (190 V) and octupole (750 V). Reference masses (m/z = 121.05 and 922 for positive mode; 112.98 and 966.00 for negative mode) were continuously infused during sample runs for accurate mass calibration. Pooled samples were run in consecutive iterative MS/MS injections at a constant collision energy of 25V to collect spectra for lipid library creation using Agilent LipidAnnotator and MS1 data was collected for all individual samples. Peak integration was performed using Agilent Profinder (v8.0) software and further curation and internal standard normalization was performed using in-house R scripts as described previously (Jain et al., 2022). Untargeted data is reported in units of pmol lipid/g tissue. Principal component analysis and heatmaps were generated using MetaboAnalyst (Pang et al., 2021). The first and second principal components are plotted on the x- and y-axes, respectively, and sample treatment group is indicated by color. For heatmap generation, data was pareto-scaled and the normalized intensity is indicated by color with relative increase in red and decrease in blue. The top 70 lipid features by ANOVA p-value are

plotted on the y-axis and samples are grouped by Ward clustering on the x-axis. Sample treatments are distinguished by color.

Targeted quantification of bis(monoacylglycerol)phosphates (BMPs) and phosphatidylglycerols (PGs)

Targeted BMP and PG lipid analysis was conducted on an Agilent 1290 Infinity II LC coupled to an Agilent 6495C QQQ mass spectrometer. The same column, mobile phases, and gradient were used for targeted analysis as for the untargeted. The MS parameters for both ionizations were as follows: drying gas temp flow of 12 L/min at 250°C with nebulizer at 35 psi and sheath gas flow of 11L/min at 300°C. Capillary voltage was kept at 4000 V with nozzle voltage of 500 V and collision energy = 20 V. The iFunnel high pressure RF was at 150/90 V and low-pressure RF at 60/60 V for positive/negative ionizations, respectively. A sample type specific lipid library was created by running pooled liver extract multiple times in positive ionization using multiple reaction monitoring (MRM) to scan for a list of BMP/PG lipid precursor masses ($[NH4]^{+}$ adducts) with transitions for the respective fatty acid and diacylglycerol (minus 17 m/z) adducts (Grabner et al., 2020). BMPs were identified by the characteristic free fatty acid fragment being much higher intensity than the diacylglycerol fragment, whereas the opposite was true for PG. In addition, BMP lipids eluted between 0.3-0.5 min earlier than the isomeric PG counterpart. These distinguishing characteristics were validated using commercial BMP 18:1_18:1 and PG 18:1_18:1 standards. A dynamic MRM method was created using the retention time data gathered from positive ionization tests but in negative mode scanning for the $[M-H]^{-}$ precursors and fatty acid fragments as BMP and PG are much more readily ionized in negative mode. Data was integrated in Agilent Quantitative analysis and peaks were manually adjusted and verified. Final units are in ng lipid/mg tissue.

Lysosome protein degradation activity assay

Lysosome protein degradation activity was performed as previously described (Robinet et al., 2021). Briefly, DQ-ovalbumin (D12053, Thermofisher Scientific) was labeled with Alexa Fluor 647 succinimidyl ester (A20006, Thermofisher Scientific) at room temperature for 1 h (3:1 dye:protein mole ratio) to make lysosome protein degradation indicator. The reaction was stopped by incubating the conjugate with 1.5 M hydroxylamine (pH 8.5) for 1h at room temperature, and the conjugate was purified by extensive dialysis. Lysosome protein degradation indicator was validated in vitro by incubating with proteinase K and achieving significant increase of Bodipy/Alexa647 ratio (Robinet et al., 2021). The double labeled ovalbumin has increased Bodipy fluorescence upon its degradation by decreasing its self-quenching, while Alexa647 is not changed upon its degradation and is used to normalize for cellular uptake. Wild type or MBOAT7Δ-Huh7 hepatoma cells treated with or without 100 mM ethanol for 48 h were incubated with 10 µg/mL of lysosome indicator for 2 h, and lysosome activity was analyzed by flow cytometry in ≈10,000 cells with a LSRFortessa device (BD). Flowjo software was used to export data for each cell for ratiometric analyses, and the median Bodipy/Alexa647 ratio for each independent well was used for analysis.

Statistical analyses

Single comparisons between two groups were performed using two-tailed Student's t tests with 95% confidence intervals. Comparisons involving multiple groups beyond binary comparison were assessed using One-way ANOVA with Tukey's post-hoc test. All data presented as mean ± SEM. Values were considered significant at $p < 0.05$ (using superscripts), or ***$p<0.001$ and ****$p<0.0001$ in figure 1. JMP 17.0 statistical discovery software (SAS Institute, Cary, NC, USA) was used for all statistical analyses.

ACKNOWLEDGEMENTS

This work was supported in part by National Institutes of Health grants P50 AA024333 (J.D., S.D., D.S.A., L.E.N., J.M.B.), R01 DK120679 (J.M.B.), RF1 NS133812 (J.M.B.), P01 HL147823 (J.M.B.), U01 AA026938 (L.E.N., J.M.B.), R01 DK130227 (J.M.B.), U01 AA026264 (L.E.N.), R01 HL128268 (J.D.S.), JDRF JDRF201309442 (J.S.), the Glenn and AFAR Junior Faculty Grant A22068 (J.S.), R01 DK133479 (J.S.); Hatch Grant WIS04000 (R.J., J.S.), K01 DK128022 (R.N.H.), and UL1TR001998 (R.N.H.). The authors would like to thank Dr. Philip Hawkins (Babraham Institute) for providing *Mboat7* knockout first mice.

COMPETING FINANCIAL INTERESTS

All other authors declare no competing financial interests related to this work.

AUTHOR CONTRIBUTIONS

V.V. and J.M.B. planned the project, designed experiments, and analyzed data. V.V. and J.M.B. wrote the original draft of the manuscript; L.E.N., J.D.S., O.R., and J.S. helped design experiments and provided useful discussion directing collaborative aspects of the project; V.V., I.R., W.J.M., R.J., R.B., A.J.H. 3rd, M.R.M., E.H., A.B., S.W.L., K.G., R.N.H., I.J., V.P., J.D., N.W., S.D., O.R., D.S., and D.S.A. either conducted mouse experiments, performed biochemical workup of mouse tissues or analyzed data and aided in manuscript preparation. All authors were involved in the editing of the final manuscript.

DATA AVAILABILITY

All materials, methods, and datasets included in this manuscript are readily available upon request.

LITERATURE CITED:

Alharthi J, Bayoumi A, Thabet K, Pan Z, Gloss BS, Latchoumanin O, Lundberg M, Twine NA, McLeod D, Alenizi S, Adams LA, Weltman M, Berg T, Liddle C, George J, Eslam M. 2022. A metabolic associated fatty liver disease risk variant in MBOAT7 regulates toll like receptor induced outcomes. *Nat. Commun.* **13:**7430.

Anderson KE, Kielkowska A, Durrant TN, Juvin V, Clark J, Stephens LR, Hawkins PT. 2013. Lysophosphatidylinositol-acyltransferase-1 (LPIAT1) is required to maintain physiological levels of PtdIns and PtdInsP(2) in the mouse. *PLoS One* **8:**e58425.

Baba, T., and T. Balla. 2020. Emerging roles of phosphatidylinositol 4-phosphate and phosphatidylinositol 4,5-bisphosphate as regulators of multiple steps in autophagy. *J. Biochem.* **168:**329-336.

Bala S, Szabo G. 2018. TFEB, a master regulator of lysosome biogenesis and autophagy, is a new player in alcoholic liver disease. *Dig. Med. Res.* **1:**16.

Beaudoin JJ, Liang T, Tang Q, Banini BA, Shah VH, Sanyal AJ, Chalasani NP, Gawrieh S. 2021. Role of candidate gene variants in modulating the risk and severity of alcoholic hepatitis. *Alcohol Clin. Exp. Res*. **45:**709-719.

Bertola A, Mathews S, Ki SH, Wang H, Gao B. 2013. Mouse model of chronic and binge ethanol feeding (the NIAAA model). *Nat. Protoc.* **8**:627-637.

Buch S, Stickel F, Trepo E, Way M, Herrmann A, Nischalke HD, Brosch M, Rosendahl J, Berg T, Ridinger M, Rietschel M, McQuillin A, Frank J, Kiefer F, Schreiber S, Lieb W, Soyka M, Semmo N, Aigner E, Datz C, et al. 2015. A genome-wide association study confirms PNPLA3 and identifies TM6SF2 and MBOAT7 as risk loci for alcohol-related cirrhosis. *Nat. Genet.* **47:**1443-1448.

Chao X, Wang S, Zhao K, Li Y, Williams JA, Li T, Chavan H, Krishnamurthy P, He XC, Li L, Ballabio A, Ni HM, Ding WX. 2018. Impaired TFEB-mediated lysosome biogenesis and autophagy promote chronic ethanol-induced liver injury and steatosis in mice. *Gastroenterology* **155:**865-879.

Clausen BE, Burkhardt C, Reith W, Renkawitz R, Förster I. 1999. Conditional gene targeting in macrophages and granulocytes using LysMcre mice. *Transgenic Res.* **8:**265-277.

Clark, J., K.E. Anderson, V. Juvin, T.S. Smith, F. Karpe, M.J. Wakelam, L.R. Stephens, and P.T. Hawkins. 2011. Quantification of PtdInsP3 molecular species in cells and tissues by mass spectrometry. *Nat. Methods* **8:**267-272.

Cohen JC, Horton JD, Hobbs, HH. 2011. Human fatty liver disease: old questions and new insights. *Science* **332:**1519-1523.

Fleming MF, Barry KL, MacDonald R. 1991. The alcohol use disorders identification test (AUDIT) in a college sample. *Int. J. Addict.* **26:**1173-1185.

Fruman, D.A., H. Chiu, B.D. Hopkins, S. Bagrodia, L.C. Cantley, and R.T. Abraham. 2017 The

PI3K pathway in human disease. *Cell* **170:**605-635.

Gijón MA., Riekhof WR, Zarini S, Murphy RC, Voelker DR. 2008. Lysophospholipid acyltransferases and arachidonate recycling in human neutrophils. *J. Biol. Chem.* **283:**30235-30245.

Grabner GF, Fawzy N, Pribasnig MA, Trieb M, Taschler U, Holzer M, Schweiger M, Wolinski H, Kolb D, Horvath A, Breinbauer R, Rülicke T, Rabl R, Lass A, Stadlbauer V, Hutter-Paier B, Stauber RE, Fickert P, Zechner R, Marsche G, Eichmann TO, Zimmermann R. 2019. Metabolic disease and ABHD6 alter the circulating bis(monoacylglycerol)phosphate profile in mice and humans. *J. Lipid Res.* **60:**1020-1031.

Gromovsky, A.D., Schugar RC, Brown AL, Helsley RN, Burrows AC, Ferguson D, Zhang R, Sansbury BE, Lee RG, Morton RE, Allende DS, Parks JS, Spite M, Brown JM. 2017. Δ-5 Fatty Acid Desaturase FADS1 Impacts Metabolic Disease by Balancing Proinflammatory and Proresolving Lipid Mediators. Δ-5 fatty acid desaturase FADS1 impacts metabolic disease by balancing proinflammatory and proresolving lipid mediators. *Arterioscler. Thromb. Vasc. Biol.* **38:**218-231.

Gruenberg J. 2020. Life in the lumen: The multivesicular endosome. *Traffic* **21:**76-93.

Helsley RN, Varadharajan V, Brown AL, Gromovsky AD, Schugar RC, Ramachandiran I, Fung K, Kabbany MN, Banerjee R, Neumann CK, Finney C, Pathak P, Orabi D, Osborn LJ, Massey W, Zhang R, Kadam A, Sansbury BE, Pan C, Sacks J, et al. 2019. Obesity-linked suppression of membrane-bound O-acyltransferase 7 (MBOAT7) drives non-alcoholic fatty liver disease. *Elife* **8:**e49882.

Hoxhaj, G., and B.D. Manning. 2020. The PI3K-AKT network at the interface of oncogenic signaling and cancer metabolism. *Nat. Rev. Cancer* **20:**74-88.

Hullin-Matsuda F, Taguchi T, Greimel P, Kobayashi T. 2014. Lipid compartmentalization in the endosome system. *Semin. Cell. Dev. Biol.* **31:**48-56.

Jain R, Wade G, Ong I, Chaurasia B, Simcox J. 2022. Determination of tissue contributions to the circulating lipid pool in cold exposure via systematic assessment of lipid profiles. *J. Lipid Res*. **63:**100197.

Krawczyk, M., M. Rau, J. M. Schattenberg, H. Bantel, A. Pathil, M. Demir, J. Kluwe, T. Boettler, F. Lammert, A. Geier, and N. C. S. Group. 2017. Combined effects of the PNPLA3 rs738409, TM6SF2 rs58542926, and MBOAT7 rs641738 variants on NAFLD severity: a multicenter biopsy-based study. *J. Lipid Res.* **58:**247-255.

Mancina RM, Dongiovanni P, Petta S, Pingitore P, Meroni M, Rametta R, Boren J, Montalcini T, Pujia A, Wiklund O, Hindy G, Spagnuolo R, Motta BM, Pipitone RM, Craxi A, Fargion S, Nobili V, Kakela P, Karja V, Mannisto V, et al. 2016. The MBOAT7-TMC4 Variant rs641738 Increases Risk of Nonalcoholic Fatty Liver Disease in Individuals of European Descent. *Gastroenterology* **150:**1219-1230.

Massey WJ, Varadharajan V, Banerjee R, Brown AL, Horak AJ, Hohe RC, Jung BM, Qiu Y, Chan ER, Pan C, Zhang R, Allende DS, Willard B, Cheng F, Lusis AJ, Brown JM. 2023.

MBOAT7-driven lysophosphatidylinositol acylation in adipocytes contributes to systemic glucose homeostasis. J*. Lipid Res.* **18:**100349.

Meroni MP. Dongiovanni M, Longo M, Carli F, Baselli G, Rametta R, Pelusi S, Badiali S, Maggioni M, Gaggini M, Fracanzani AL, Romeo S, Gatti S, Davidson NO, Gastaldelli A, Valenti L. 2020. Mboat7 down-regulation by hyper-insulinemia induces fat accumulation in hepatocytes. *EBioMedicine* **52:**102658.

Pang Z, Chong J, Zhou G, de Lima Morais DA, Chang L, Barrette M, Gauthier C, Jacques PÉ, Li S, Xia J. 2021. MetaboAnalyst 5.0: narrowing the gap between raw spectra and functional insights. *Nucleic Acids Res*. **49(W1):**W388-W396.

Pemberton, J.G., Y.J. Kim, and T. Balla. 2020. Integrated regulation of phosphatidylinositol cycle and phosphoinositide-driven lipid transport at ER-PM contact sites. *Traffic* **21:** 200-219.

Postic C, Shiota M, Niswender KD, Jetton TL, Chen Y, Moates JM, Shelton KD, Lindner J, Cherrington AD, Magnuson MA. 1999. Dual roles for glucokinase in glucose homeostasis as determined by liver and pancreatic beta cell-specific gene knock-outs using Cre recombinase. *J. Biol. Chem.* **274:**305-315.

Rinella ME, Sanyal AJ. 2016. Management of NAFLD: a stage-based approach. *Nat. Rev. Gastroenterol. Hepatol.* **13:**196-205.

Robinet P, Ritchey B, Lorkowski SW, Alzayed AM, DeGeorgia S, Schodowski E, Traughber CA, Smith JD. 2021. Quantitative trait locus mapping identifies the Gpnmb gene as a modifier of mouse macrophage lysosome function. Sci Rep. **11**:10249.

Rouzer, C.A., P.T. Ivanova, M.O. Byrne, H.A. Brown, and L.J. Marnett. 2007. Lipid profiling reveals glycerophospholipid remodeling in zymosan-stimulated macrophages. *Biochemistry* **46:**6026-6042.

Sabatine MS. 2019. PCSK9 inhibitors: clinical evidence and implementation. *Nat. Rev. Cardiol.* 16: 155-165.

Samuel VT, Shulman GI. 2018. Nonalcoholic fatty liver disease as a nexus of metabolic and hepatic diseases. *Cell Metab.* **27:**22-41.

Schink, K.O., K.W. Tan, and H. Stenmark. 2016. Phosphoinositides in control of membrane dynamics. *Annu. Rev. Cell. Dev. Biol*. **32:**143-171.

Schugar R, Shih DM, Warrier M, Helsley RN, Burrows A, Ferguson D, Brown AL, Gromovsky AD, Heine M, Chatterjee A, Li L, Li XS, Wang Z, Willard B, Meng Y, Kim H, Che N, Pan C, Lee RG, Crooke RM, Graham MJ, Morton RE, Langefeld CD, Das SK, Rudel LL, Zein N, McCullough AJ, Dasarathy S, Tang WHW, Erokwu BO, Flask CA, Laakso M, Civelek M, Naga Prasad SV, Heeren J, Lusis AJ, Hazen SL, Brown JM. 2017. The TMAO-producing enzyme flavin-containing monooxygenase 3 regulates obesity and the beiging of white adipose tissue. *Cell Rep.* **19:**2451-2461.

Shindou, H., and T. Shimizu. 2009. Acyl-CoA:lysophospholipid acyltransferases. *J. Biol. Chem*. **284:**1-5.

Showalter MR, Berg AL, Nagourney A, Heil H, Carraway KL 3rd, Fiehn O. 2020. The emerging and diverse roles of bis(monoacylglycero) phosphate lipids in cellular physiology and disease. *Int. J. Mol. Sci.* **21:**8067.

Stickel F, S. Buch HD, Nischalke, KH, Weiss D, Gotthardt J, Fischer J, Rosendahl A, Marot M, Elamly M, Casper F, Lammert A, McQuillin S, Zopf U, Spengler S, Marhenke MM, Kirstein A, Vogel F, Eyer J, von Felden H, Wege T, Buch C, Schafmayer F, Braun P, Deltenre T, Berg M, Morgan Y, Hampe J. 2018. Genetic variants in PNPLA3 and TM6SF2 predispose to the development of hepatocellular carcinoma in individuals with alcohol-related cirrhosis. *Am. J. Gastroenterol.* **113:**1475-1483.

TanakaY, Shimanaka Y, Caddeo A, Kubo T, Mao Y, Kubota T, Kubota N, Yamauchi T, Mancina RM, Baselli G, Luukkonen P, Pihlajamäki J, Yki-Järvinen H, Valenti L, Arai H, Romeo S, Kono N. 2021. LPIAT1/MBOAT7 depletion increases triglyceride synthesis fueled by high phosphatidylinositol turnover. *Gut* **70:**180-193.

Teo K, Abeysekera KWM, Adams L, Aigner E, Anstee QM, Banales JM, Banerjee R, Basu P, Berg T, Bhatnagar P, Buch S, Canbay A, Caprio S, Chatterjee A, Ida Chen JD, Chowdhury A, Daly AK, Datz C, de Gracia Hahn D, DiStefano JK, et al. 2021. rs641738C>T near MBOAT7 is associated with liver fat, ALT and fibrosis in NAFLD: A meta-analysis. *J. Hepatol.* **74:**20-30.

Thabet K, Asimakopoulos A, Shojaei M, Romero-Gomez M, Mangia A, Irving WL, Berg T, Dore GJ, Gronbaek H, Sheridan D, Abate ML, Bugianesi E, Weltman M, Mollison L, Cheng W, Riordan S, Fischer J, Spengler U, Nattermann J, Wahid A, et al. 2016. MBOAT7 rs641738 increases risk of liver inflammation and transition to fibrosis in chronic hepatitis C. *Nat. Commun.* **7:**12757.

Thabet K, Chan HLY, Petta S, Mangia A, Berg T, Boonstra A, Brouwer WP, Abate ML, Wong VW, Nazmy M, Fischer J, Liddle C, George J, Eslam M. 2017. The membrane-bound O-acyltransferase domain-containing 7 variant rs641738 increases inflammation and fibrosis in chronic hepatitis B. *Hepatology* **65:**1840-1850.

Thangapandi VR, Knittelfelder O, Brosch M, Patsenker E, Vvedenskaya O, Buch S, Hinz S, Hendricks A, Nati M, Herrmann A, Rekhade DR, Berg T, Matz-Soja M, Huse K, Klipp E, Pauling JK, Wodke JA, Miranda Ackerman J, Bonin MV, Aigner E. et al. 2021. Loss of hepatic *Mboat7* leads to liver fibrosis. *Gut* **70:** 940-950.

Warrier, M., Warrier M, Shih DM, Burrows AC, Ferguson D, Gromovsky AD, Brown AL, Marshall S, McDaniel A, Schugar RC, Wang Z, Sacks J, Rong X, Vallim TA, Chou J, Ivanova PT, Myers DS, Brown HA, Lee RG, Crooke RM, Graham MJ, Liu X, Parini P, Tontonoz P, Lusis AJ, Hazen SL, Temel RE, Brown JM. 2015. The TMAO-Generating Enzyme Flavin Monooxygenase 3 Is a Central Regulator of Cholesterol Balance. *Cell Rep.* **10:**1-13.

Wymann, M.P., and R. Schneiter. 2008. Lipid signaling in disease. *Nat. Rev. Mol. Cell Biol.* **9:**162-176.

Xia M, Chandrasekaran P, Rong S, Fu X, Mitsche MA. 2021. Hepatic deletion of *Mboat7* (LPIAT1) causes activation of SREBP-1c and fatty liver. *J. Lipid Res.* **62:**100031.

Zarini S, Hankin JA, Murphy RC, Gijón MA. 2014. Lysophospholipid acyltransferases and arachidonate recycling in human neutrophils. *Prostaglandins Other Lipid Mediat*. **113-115:**52-61.

Zhang, Y., T. Guo, F. Yang, Y. Mao, L. Li, C. Liu, Q. Sun, Y. Li, and J. Huang. 2018. Single nucleotide rs738409 polymorphisms in the PNPLA3 gene are strongly associated with alcoholic liver disease in Han Chinese males. *Hepatol. Int.* **12:** 429-437.

FIGURE LEGENDS

Figure 1. MBOAT7 Products Are Selectively Reduced in Heavy Drinkers. Plasma lysophosphatidylinositol (LPI - inset graph) and phosphatidylinositol (PI) species from both male and female healthy controls and heavy drinkers were measured by liquid chromatography-tandem mass spectrometry (LC-MS/MS). n=10-16; ***p<0.001 and ****p<0.0001 in figure 1. ANOVA with Tukey's post-hoc test.

Figure 1 – figure supplement 1. Demographic and clinical parameters for the entire cohort of healthy controls and heavy drinkers recruited for this study.

Figure 2. Hepatocyte-Specific Deletion of *Mboat7* Promotes Ethanol-Induced Liver Injury. Female control (*Mboat7*$^{fl/fl}$) or hepatocyte-specific *Mboat7* knockout mice (*Mboat7*^{HSKO}) were fed with subjected the NIAAA model of ethanol-induced liver injury. (A) Hepatic *Mboat7* expression was measured via qPCR. (B) Western blot for hepatic microsomal MBOAT7 protein levels replicated in n=3 mice. (C) Liver weight, (D) Plasma alanine aminotransferase (ALT), (E) Percent steatosis quantified by a blinded board-certified pathologist, (F) Hepatic triglycerides, (G) Hepatic expression of Inflammatory gene measured by qPCR. n = 5-7; Data represent the mean ± S.E.M. and groups not sharing a common letter superscript differ significantly (p p≤0.05).

Figure 2 – figure supplement 1. Myeloid-Specific Deletion of *Mboat7* Does not Promote Ethanol-Induced Liver Injury. Female control (Mboat7$^{fl/fl}$) or myeloid-specific *Mboat7* knockout mice (*Mboat7*^{MSKO}) were subjected to the NIAAA model of ethanol-induced liver injury. (A) Western blots from bone marrow derived macrophage (BMDM) or peritoneal macrophage (PM) collected from *Mboat7*$^{fl/fl}$ or *Mboat7*^{HSKO} mice. (B) Initial and final Body weight measured in

Mboat7$^{fl/fl}$ or *Mboat7*^{MSKO} mice. (C) Liver weight (D and E) Plasma alanine aminotransferase (ALT) and aspartate aminotransferase (AST). (F) Hepatic triglycerides. (G) Hepatic expression of Inflammatory gene measured by qPCR. Data represent the mean ± S.E.M. and groups not sharing a common letter superscript differ significantly (p p≤0.05).

Figure 3. Ethanol Alters the Liver Lipidome in a MBOAT7-Dependent Manner. *Mboat7*$^{fl/fl}$ or *Mboat7*^{HSKO} mice were subjected to the NIAAA model of ethanol exposure. Liver lysophosphatidylinositol (LPI) (A) and phosphatidylinositol (PI) species, including the MBOAT7 product PI 38:4 (B) and others (C), were quantified via liquid chromatography-tandem mass spectrometry (LC-MS/MS) in (n=5-7). (D) Principal component analysis for untargeted lipidomics analysis. The first and second principal components are plotted on the x- and y-axes, respectively, and sample treatment group is indicated by color. (E) Heatmap showing global lipidomic alterations in mouse liver. Total levels of endosomal/lysosomal lipids were measured by targeted and untargeted lipidomic approach using LC-MS/MS (F) Total Bis(monoacylglycero)phosphate (BMP) levels (G) Total Phosphatidylglycerol (PG) and (H) Total Cardiolipin (CL) from the liver of Mboat7$^{fl/fl}$ or Mboat7^{HSKO} mice. Data represent the mean ± S.E.M. and groups not sharing a common letter superscript differ significantly (p p≤0.05).

Figure 3 – figure supplement 1. Alterations in Total Hepatic Lipid Levels in *Mboat7*^{HSKO} Mice*.* Age-matched female *Mboat7*$^{fl/fl}$ or *Mboat7*^{HSKO} mice were subjected to the NIAAA model of ethanol exposure, and untargeted lipidomics was performed to broadly examine major lipid classes in the liver. (A) Phosphatidylcholine (PC), (B) Phosphatidylserine (PS), (C) Phosphatidylethanolamine (PE), (D) Phosphatidic acid (PA), (E) Sphingomyelins (SM), (F) Ceramides (Cer), (G) Ether phosphatidylcholine, (H) Ether phosphatidylethanolamine, (I) Free fatty acids (FFA), (J) Hexosylceramide (HexCer), (K) Diacylglycerol (DAG) and (L) Cholesteryl

ester (CE) were quantified via liquid chromatography mass spectrometry (n=6/group). Data represent the mean ± S.E.M. and groups not sharing a common letter superscript differ significantly (p p≤0.05).

Figure 3 – figure supplement 2. Hepatic Phosphatidylcholine (PC) Levels in *Mboat7^{HSKO}* mice. Age-matched female *Mboat7*$^{fl/fl}$ or *Mboat7*^{HSKO} mice were subjected to the NIAAA model of ethanol exposure, and untargeted lipidomics were performed to broadly examine major lipid classes in the liver. The molecular species of PC were quantified via liquid chromatography mass spectrometry (n=6/group). Data represent the mean ± S.E.M. and groups not sharing a common letter superscript differ significantly (p p≤0.05).

Figure 3 – figure supplement 3. Hepatic Bis(Monoacylglycerol)Phosphate (BMP) Levels in *Mboat7^{HSKO}* mice. Age-matched female *Mboat7*$^{fl/fl}$ or *Mboat7*^{HSKO} mice were subjected to the NIAAA model of ethanol exposure, and targeted lipidomics was performed in the liver. The molecular species of BMP were quantified via liquid chromatography mass spectrometry (n=6/group). Data represent the mean ± S.E.M. and groups not sharing a common letter superscript differ significantly (p p≤0.05).

Figure 3 – figure supplement 4. Hepatic Phosphatidylglycerol (PG) Levels in *Mboat7^{HSKO}* mice. Age-matched female *Mboat7*$^{fl/fl}$ or *Mboat7*^{HSKO} mice were subjected to the NIAAA model of ethanol exposure, and targeted lipidomics was performed in the liver. The molecular species of PG were quantified via liquid chromatography mass spectrometry (n=6/group). Data represent the mean ± S.E.M. and groups not sharing a common letter superscript differ significantly (p p≤0.05).

Figure 3 – figure supplement 5. Hepatic Cardiolipin (CL) Levels in *Mboat7^{HSKO}* mice. Age-matched female *Mboat7*$^{fl/fl}$ or *Mboat7*^{HSKO} mice were subjected to the NIAAA model of ethanol exposure, and untargeted lipidomics was performed in the liver. The molecular species of CL were quantified via liquid chromatography mass spectrometry (n=6/group). Data represent the mean ± S.E.M. and groups not sharing a common letter superscript differ significantly (p p≤0.05).

Figure 3 – figure supplement 6. Hepatic Phosphatidylserine (PS) Levels in *Mboat7^{HSKO}* mice. Age-matched female *Mboat7*$^{fl/fl}$ or *Mboat7*^{HSKO} mice were subjected to the NIAAA model of ethanol exposure, and untargeted lipidomics was performed in the liver. The molecular species of PS were quantified via liquid chromatography mass spectrometry (n=6/group). Data represent the mean ± S.E.M. and groups not sharing a common letter superscript differ significantly (p p≤0.05).

Figure 3 – figure supplement 7. Hepatic Phosphatidylethanolamine (PE) Levels in *Mboat7^{HSKO}* mice. Age-matched female *Mboat7*$^{fl/fl}$ or *Mboat7*^{HSKO} mice were subjected to the NIAAA model of ethanol exposure, and untargeted lipidomics was performed in the liver. The molecular species of PE were quantified via liquid chromatography mass spectrometry (n=6/group). Data represent the mean ± S.E.M. and groups not sharing a common letter superscript differ significantly (p p≤0.05).

Figure 3 – figure supplement 8. Hepatic Phosphatidic Acid (PA) Levels in *Mboat7^{HSKO}* mice. Age-matched female *Mboat7*$^{fl/fl}$ or *Mboat7*^{HSKO} mice were subjected to the NIAAA model of ethanol exposure, and untargeted lipidomics was performed in the liver. The molecular species of PA were quantified via liquid chromatography mass spectrometry (n=6/group). Data

represent the mean ± S.E.M. and groups not sharing a common letter superscript differ significantly (p p≤0.05).

Figure 3 – figure supplement 9. Hepatic Sphingomyelin (SM) Levels in *Mboat7*^{HSKO} mice. Age-matched female *Mboat7*$^{fl/fl}$ or *Mboat7*^{HSKO} mice were subjected to the NIAAA model of ethanol exposure, and untargeted lipidomics was performed in the liver. The molecular species of SM were quantified via liquid chromatography mass spectrometry (n=6/group). Data represent the mean ± S.E.M. and groups not sharing a common letter superscript differ significantly (p p≤0.05).

Figure 3 – figure supplement 10. Hepatic Ceramide (Cer) Levels in *Mboat7*^{HSKO} mice. Age-matched female *Mboat7*$^{fl/fl}$ or *Mboat7*^{HSKO} mice were subjected to the NIAAA model of ethanol exposure, and untargeted lipidomics was performed in the liver. The molecular species of ceramides were quantified via liquid chromatography mass spectrometry (n=6/group). Data represent the mean ± S.E.M. and groups not sharing a common letter superscript differ significantly (p p≤0.05).

Figure 3 – figure supplement 11. Hepatic Ether-Linked Lipids Levels in *Mboat7*^{HSKO} mice. Age-matched female *Mboat7*$^{fl/fl}$ or *Mboat7*^{HSKO} mice were subjected to the NIAAA model of ethanol exposure, and untargeted lipidomics was performed in the liver. The molecular species of ether-linked lipids were quantified via liquid chromatography mass spectrometry (n=6/group). Data represent the mean ± S.E.M. and groups not sharing a common letter superscript differ significantly (p p≤0.05).

Figure 4. *Mboat7*^{HSKO} Mice Have Dysregulated Lysosome Function in Response to

Ethanol. Age-matched female *Mboat7*$^{fl/fl}$ or *Mboat7*^{HSKO} mice were subjected to the NIAAA model of ethanol exposure**.** (A) Total liver lysates were subjected to western blot analysis of major autophagy marker genes (LC3A/B, P62), mTOR and lysosome biogenesis genes (TFEB, LAMP-1, LAMP-2 and ATP6V1A). (B) Nuclear fractions from mouse livers of Mboat7$^{fl/fl}$ and *Mboat7*^{HSKO} were subjected to western blot analysis of TFEB. (C) Lysosome protein degradation activity in wild type and MBOAT7Δ-Huh7 hepatoma cells treated with or without 100 mM ethanol for 48 h was assessed by incubating cells with 10 µg/mL of lysosome indicator for 2 h and examined by flow cytometry. (n=5 from two experiments by normalizing to wild type group in each experiment; mean ± S.D. (D) Expression levels of the genes encoding functions in lysosomal hydrolase and accessory, lysosomal m involved in lysosomal biogenesis in the liver of Mboat7$^{fl/fl}$ and Mboat7^{HSKO} *mice* upon ethanol feeding. mRNA expression levels were determined by qPCR. (n=6/group). Groups not sharing a common letter superscript differ significantly (p p≤0.05).

Figure 4 – figure supplement 1. Genetic Deletion of MBOAT7 in Human Huh7 Cells is Associated with Diminished Lysosome Biogenesis and Ethanol-Induced Autophagy Dysregulation. WT and *MBOAT7Δ* Huh7 hepatoma cells were treated with and without ethanol treatment (100mM) for 24 (A) and 48h (B). Total lysate were subjected to western blot analysis of LC3A/B, P62, Total mTOR, Total TFEB, LAMP-1, LAMP-2 and ATP6V1A.

Figure 4 – figure supplement 2. Working Model. MBOAT7 loss of function in either mouse or human hepatocytes is associated with decreased TFEB-driven lysosomal biogenesis and defective autophagy secondary to lysosomal dysfunction.

Figure 1

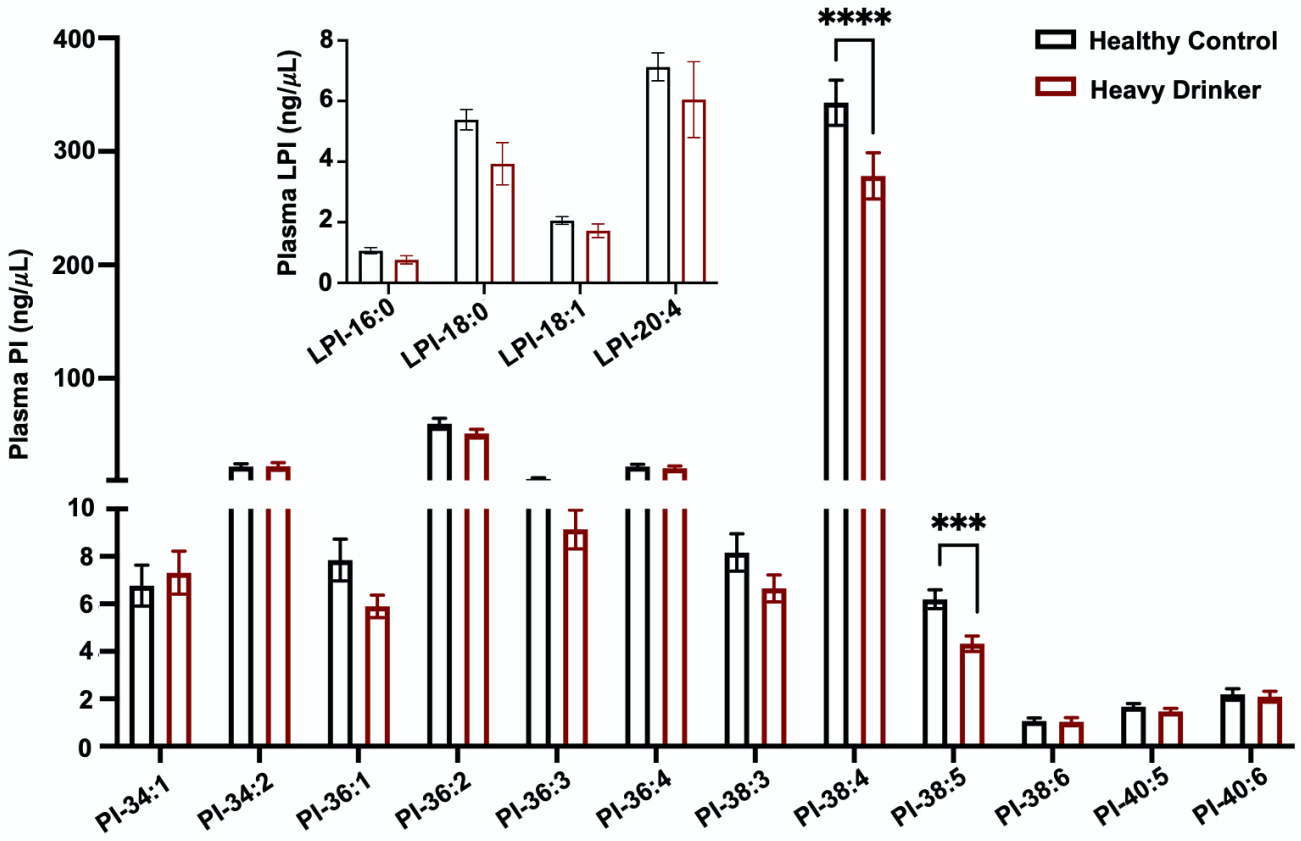
Healthy Control
Heavy Drinker
Plasma PI (ng/μL)
400
300
200
100
10
8
6
4
2
0
****
***
Plasma LPI (ng/μL)
8
6
4
2
0
LPI-16:0
LPI-18:0
LPI-18:1
LPI-20:4
PI-34:1
PI-34:2
PI-36:1
PI-36:2
PI-36:3
PI-36:4
PI-38:3
PI-38:4
PI-38:5
PI-38:6
PI-40:5
PI-40:6

Figure 1 – figure supplement 1: Clinical Demographics for Healthy vs Heavy Drinkers

	Healthy Control (N=25)	Healthy Drinker (N=21)	Total (N=46)	p value
Sex				0.88
Female	16 (64.0%)	13 (61.9%)	29 (63.0%)	
Male	9 (36.0%)	8 (38.1%)	17 (37.0%)	
Age				0.85
Mean	45.16	44.38	44.80	
Range	23.00 - 63.00	21.00 - 63.00	21.00 - 63.00	
Race				0.06
African American	5 (20.0%)	13 (61.9%)	18 (39.1%)	
Asian	1 (4.0%)	0 (0.0%)	1 (2.2%)	
Hispanic	1 (4.0%)	1 (4.8%)	2 (4.3%)	
Unknown	3 (12.0%)	1 (4.8%)	4 (8.7%)	
White	15 (60.0%)	6 (28.6%)	21 (45.7%)	
MELD				0.56
Healthy	25 (100.0%)	21 (100.0%)	46 (100.0%)	
BMI				0.03
Mean	27.12	23.83	24.74	
Range	22.12 - 30.90	15.16 - 28.59	15.16 - 30.90	
Bilirubin				0.14
Mean	0.57	0.79	0.72	
Range	0.20 - 0.90	0.10 - 1.60	0.10 - 1.60	
AST				0.51
Mean	24.56	26.52	25.93	
Range	16.00 - 38.00	15.00 - 44.00	15.00 - 44.00	
ALT				0.98
Mean	23.22	23.10	23.13	
Range	12.00 - 41.00	10.00 - 59.00	10.00 - 59.00	
Creatine				0.94
Mean	0.91	0.90	0.90	
Range	0.51 - 1.20	0.41 - 1.68	0.41 - 1.68	
INR				0.90
Mean	1.06	1.05	1.05	
Range	1.00 - 1.14	0.96 - 1.13	0.96 - 1.14	
Albumin				0.13
Mean	3.41	4.03	3.86	
Range	0.51 - 4.70	3.50 - 4.70	0.51 - 4.70	
WBC				0.02
Mean	34.17	13.51	16.95	
Range	29.40 - 41.30	1.97 - 36.50	1.97 - 41.30	
Total Protein				0.97
Mean	6.90	6.91	6.91	
Range	6.20 - 7.30	5.50 - 8.30	5.50 - 8.30	
Globulin				< 0.01
Mean	13.50	5.48	7.56	
Range	9.80 - 16.00	1.80 - 14.40	1.80 - 16.00	

Figure 2

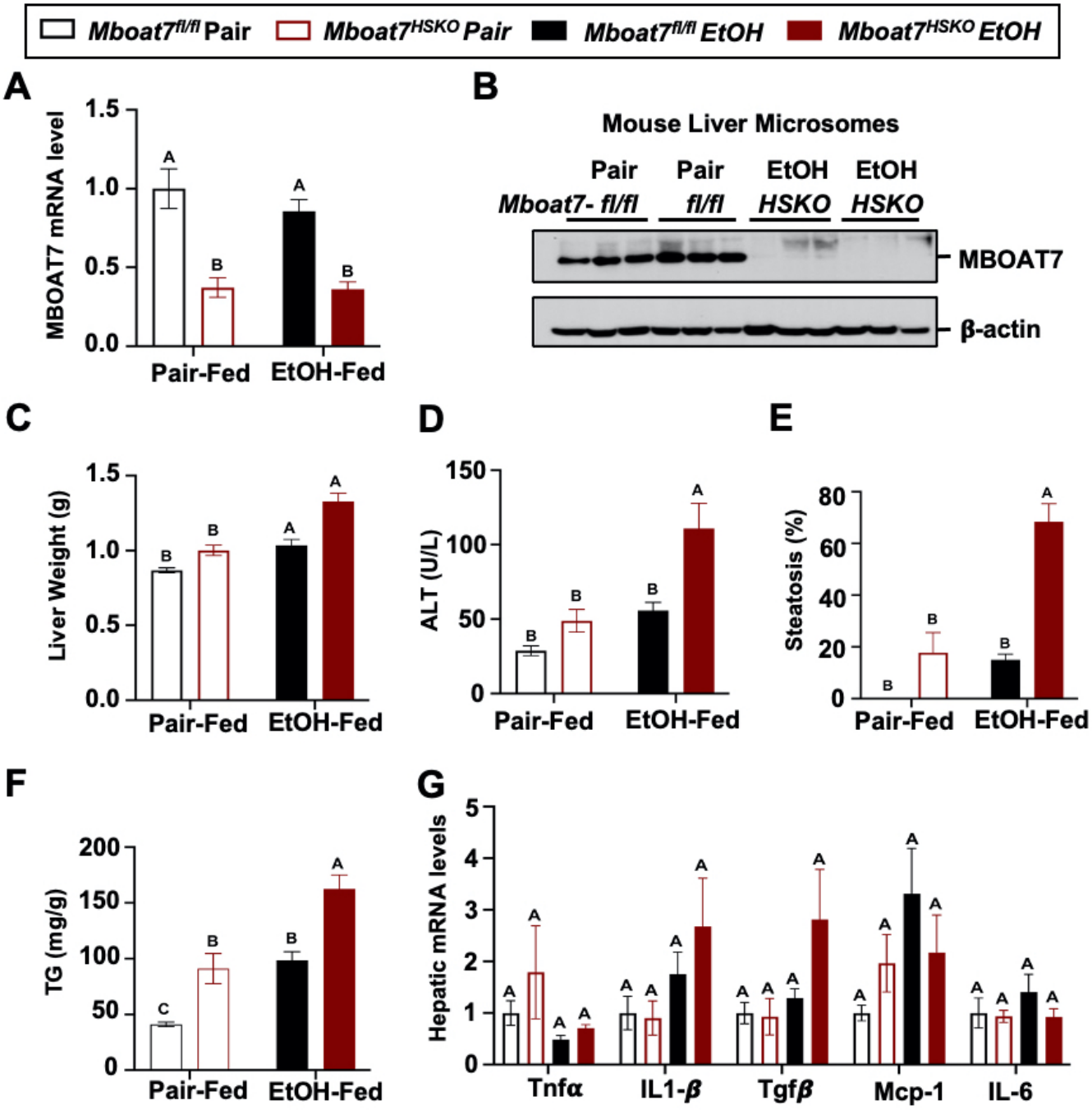
Mboat7fl/fl Pair
Mboat7HSKO Pair
Mboat7fl/fl EtOH
Mboat7HSKO EtOH
A
MBOAT7 mRNA level
1.5
1.0
0.5
0.0
Pair-Fed
EtOH-Fed
B
Mouse Liver Microsomes
Pair
Pair
EtOH
EtOH
Mboat7- fl/fl
fl/fl
HSKO
HSKO
MBOAT7
β-actin
C
Liver Weight (g)
D
ALT (U/L)
150
100
50
0
E
Steatosis (%)
80
60
40
20
F
TG (mg/g)
200
150
100
50
G
Hepatic mRNA levels
5
4
3
2
1
Tnfα
IL1-β
Tgfβ
Mcp-1
IL-6

Figure 2 – figure supplement 1

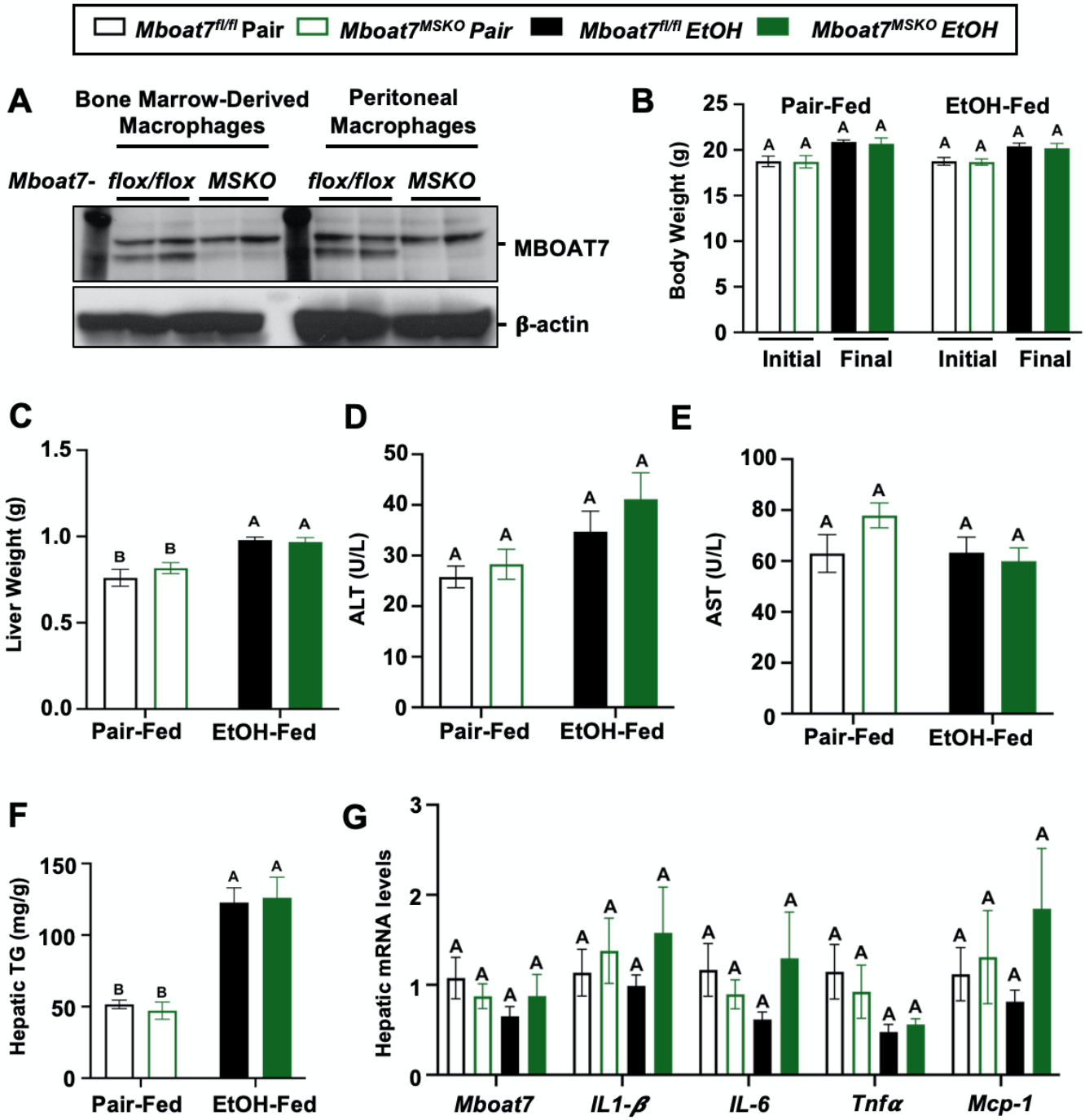

Figure 3

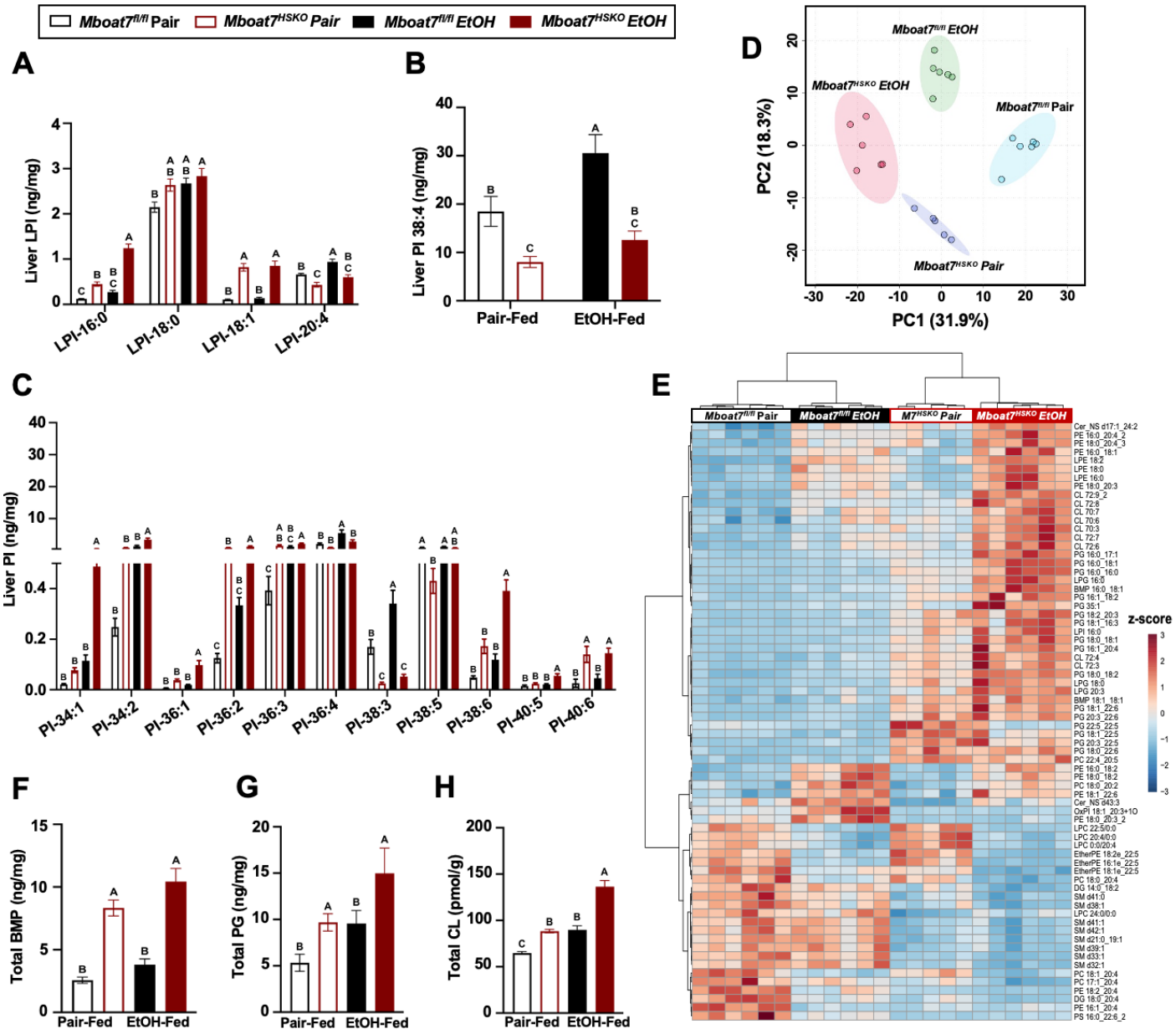
Mboat7fl/fl Pair
Mboat7HSKO Pair
Mboat7fl/fl EtOH
Mboat7HSKO EtOH
A
Liver LPI (ng/mg)
LPI-16:0
LPI-18:0
LPI-18:1
LPI-20:4
B
Liver PI 38:4 (ng/mg)
Pair-Fed
EtOH-Fed
D
PC2 (18.3%)
PC1 (31.9%)
C
Liver PI (ng/mg)
PI-34:1
PI-34:2
PI-36:1
PI-36:2
PI-36:3
PI-36:4
PI-38:3
PI-38:5
PI-38:6
PI-40:5
PI-40:6
E
M7HSKO Pair
z-score
F
Total BMP (ng/mg)
G
Total PG (ng/mg)
H
Total CL (pmol/g)

Figure 3 – Figure Supplement 1

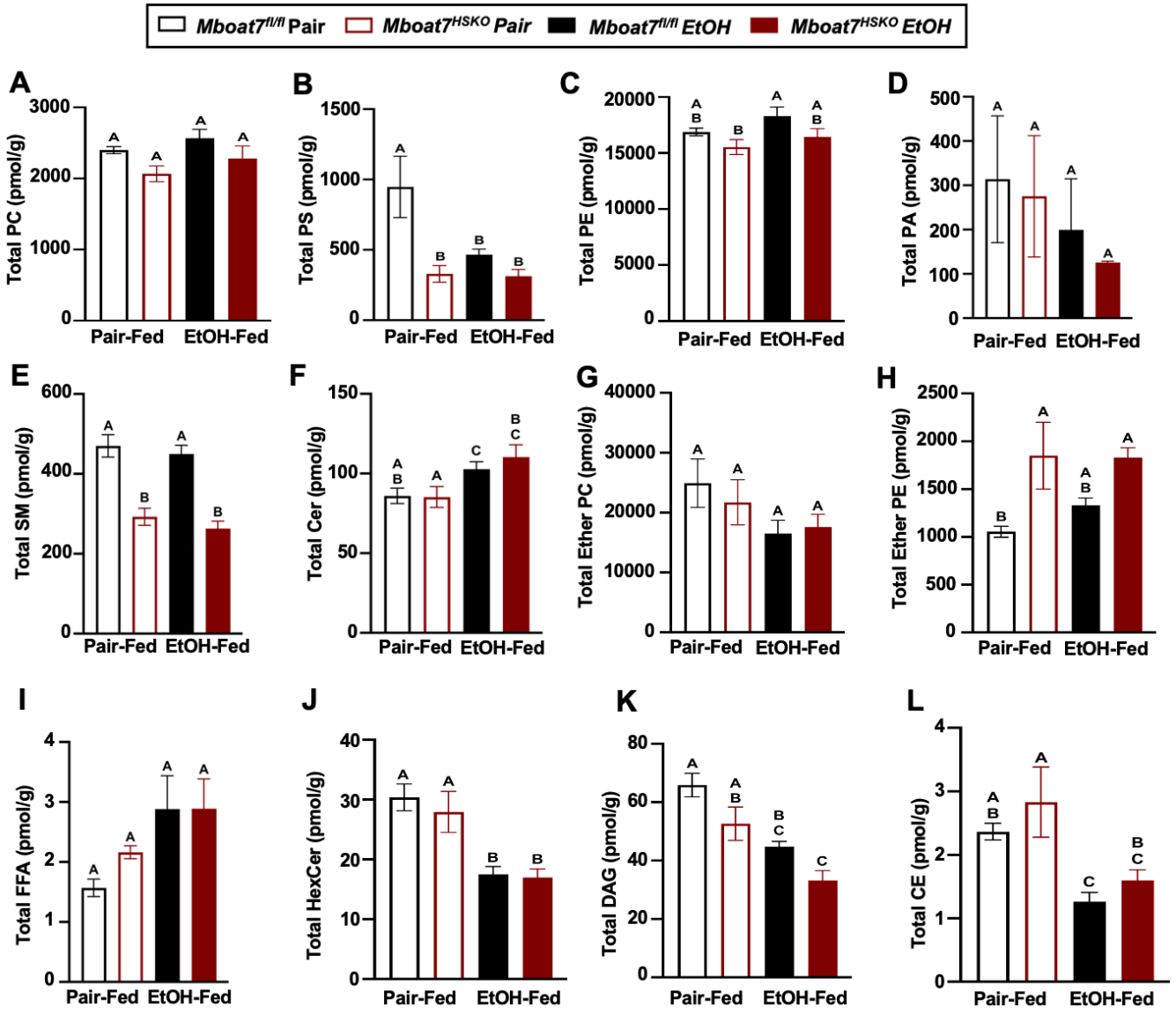

Figure 3 – Figure Supplement 2

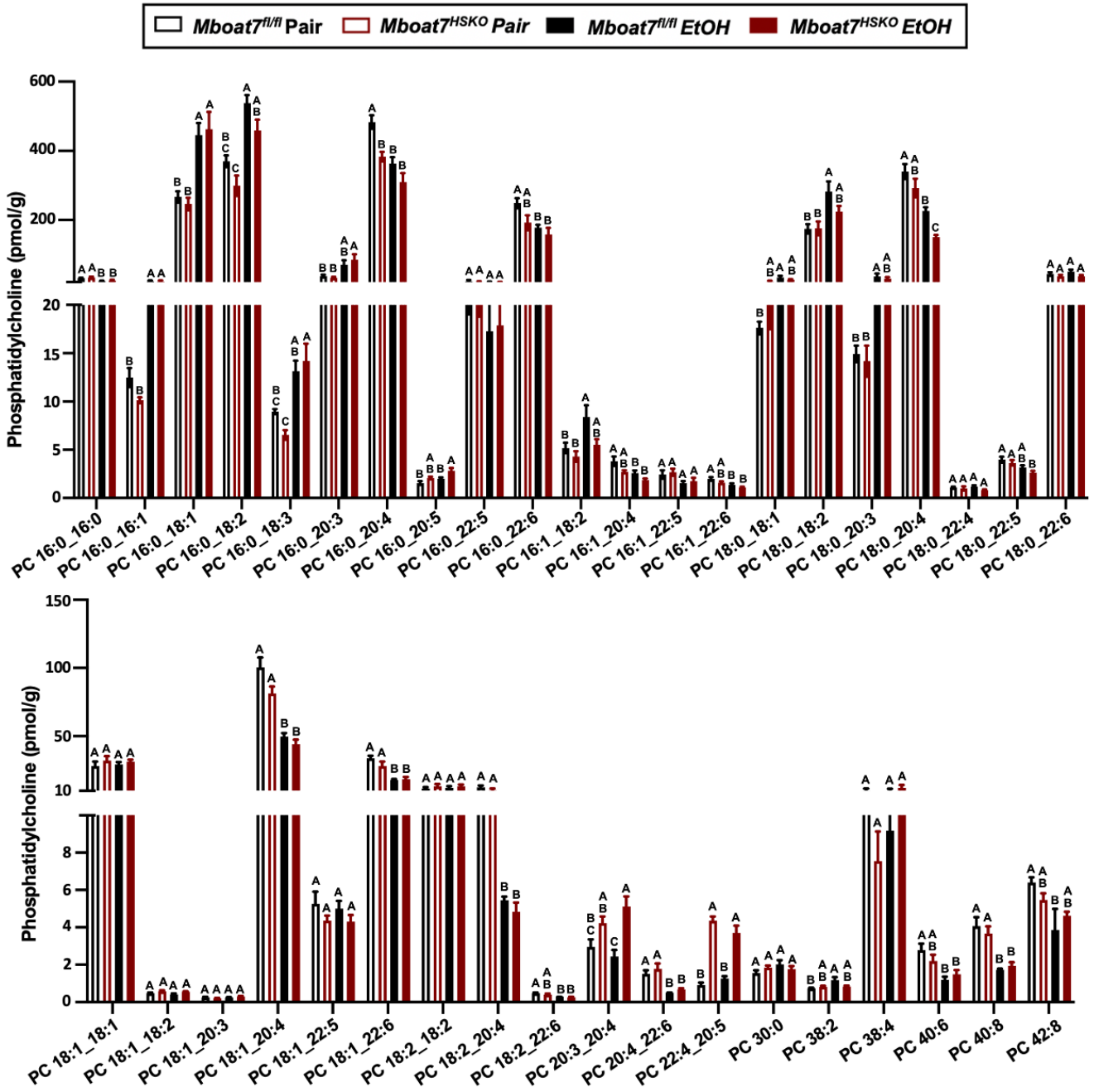

Figure 3 – Figure Supplement 2

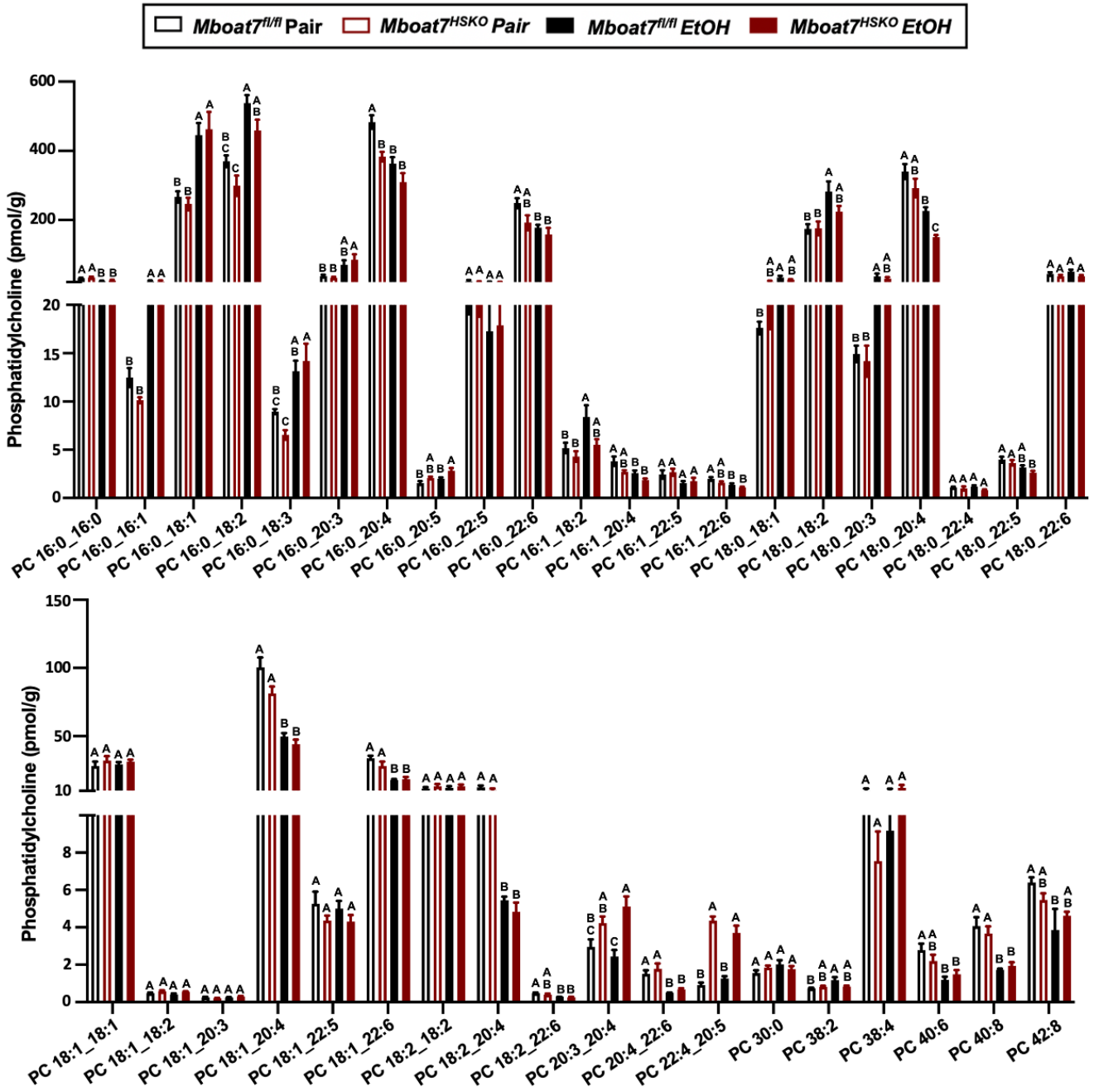

Figure 3 – Figure Supplement 3

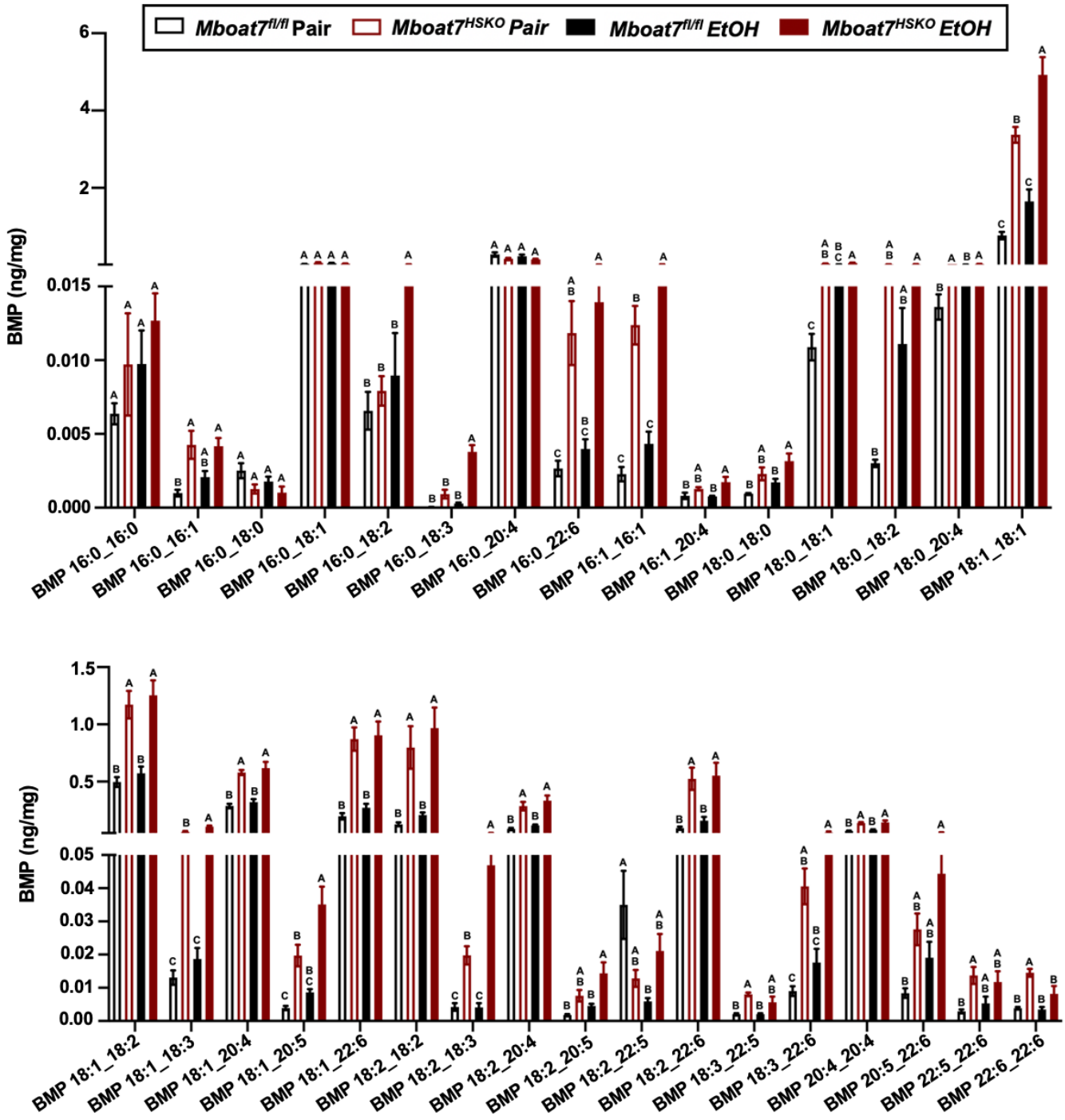

Figure 3 – Figure Supplement 4

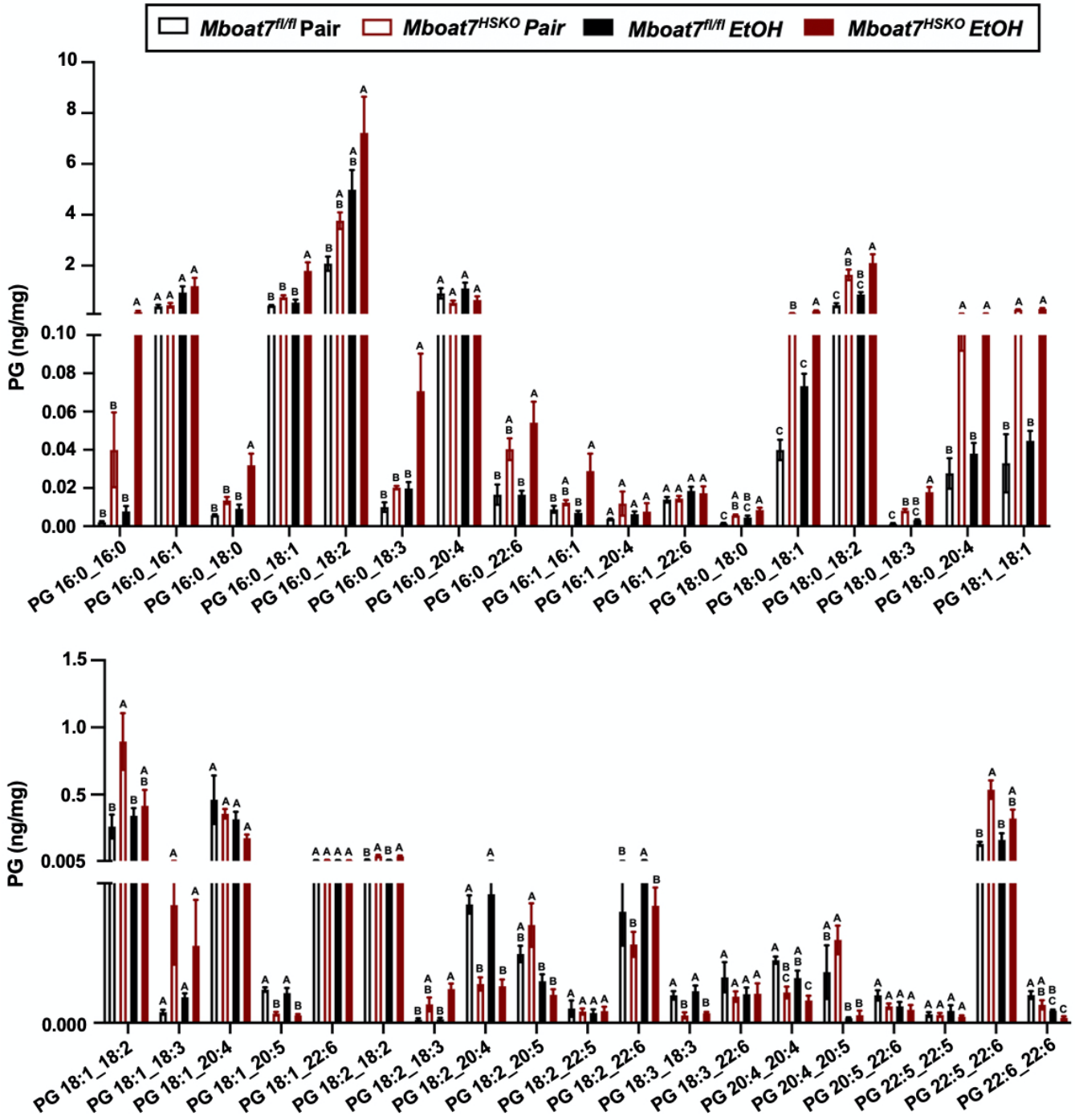

Figure 3 – Figure Supplement 5

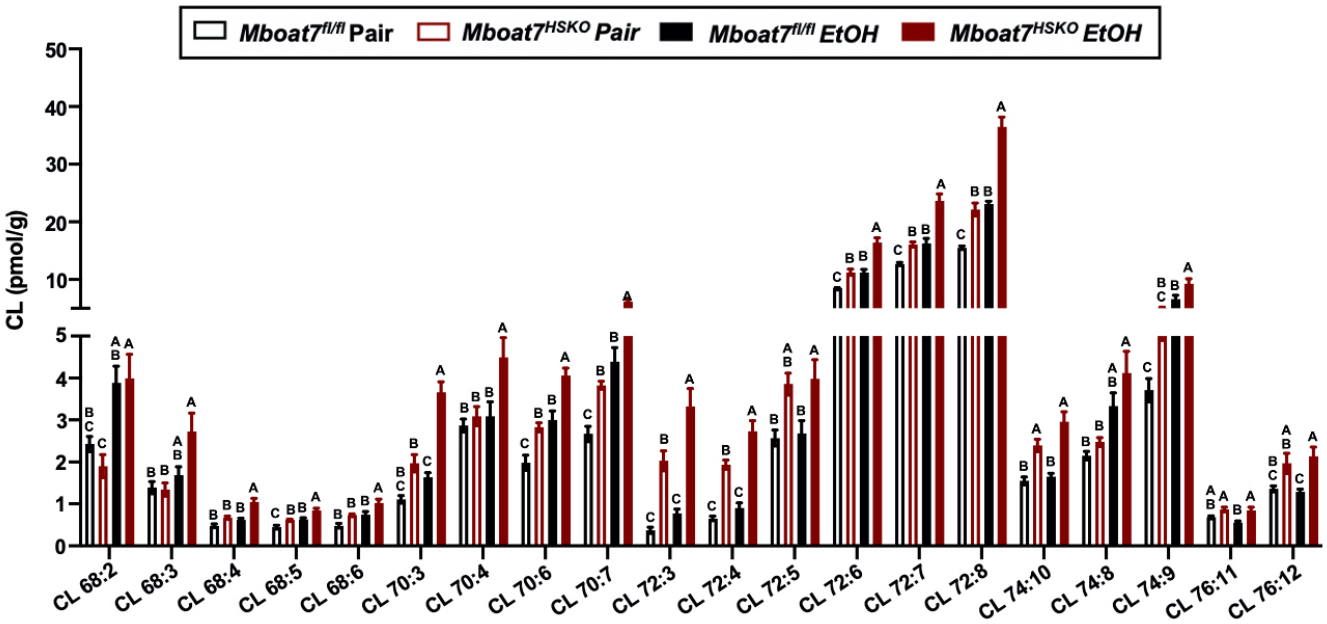

Figure 3 – Figure Supplement 6

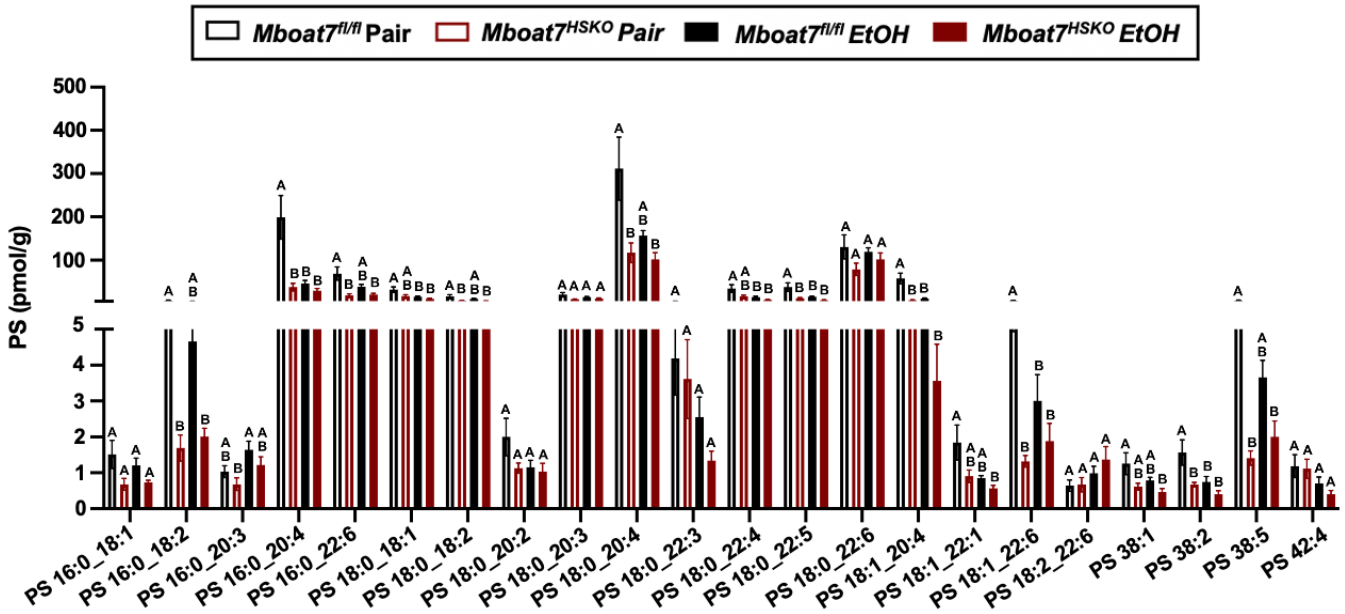

Figure 3 – Figure Supplement 7

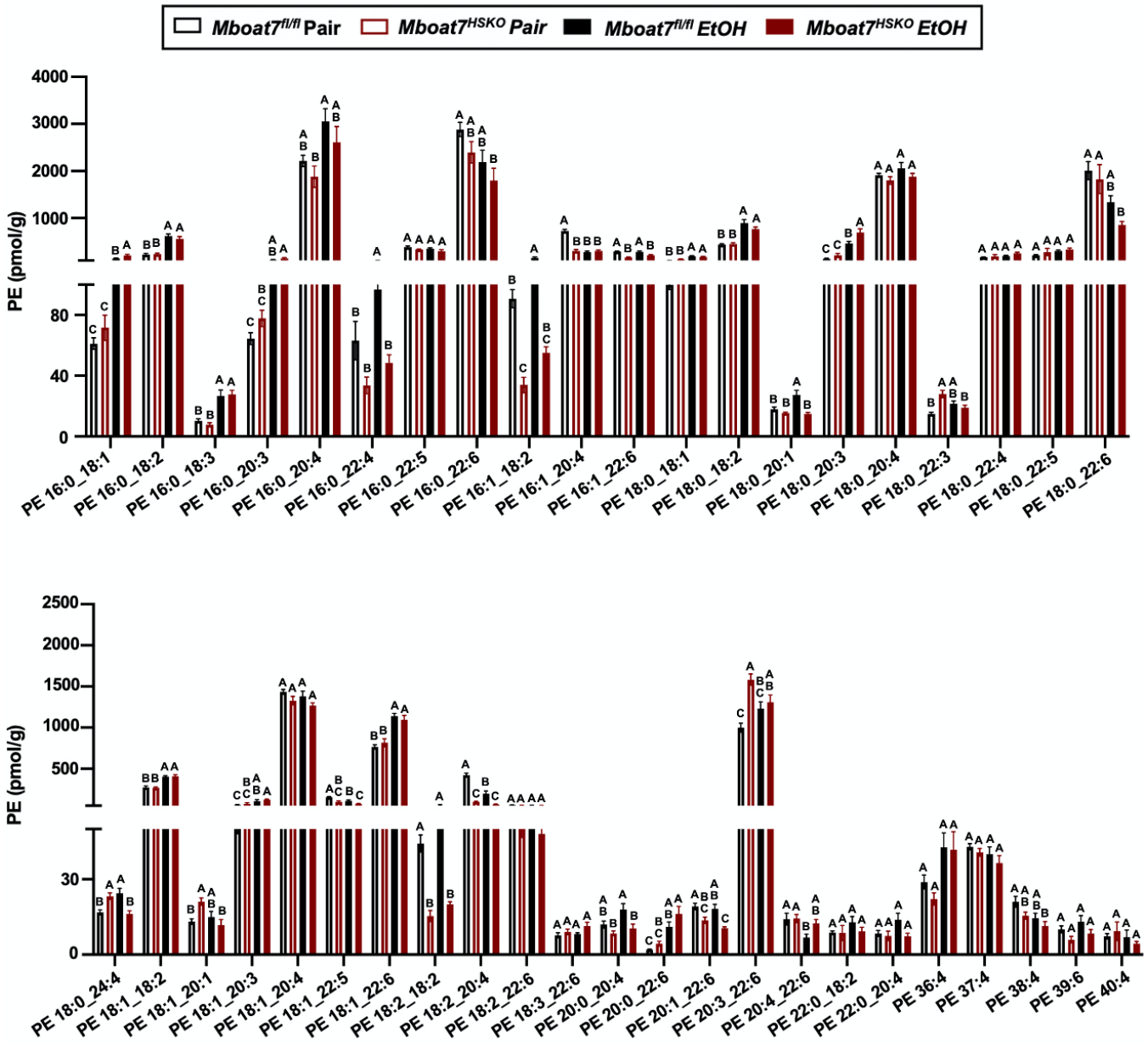

Figure 3 – Figure Supplement 8

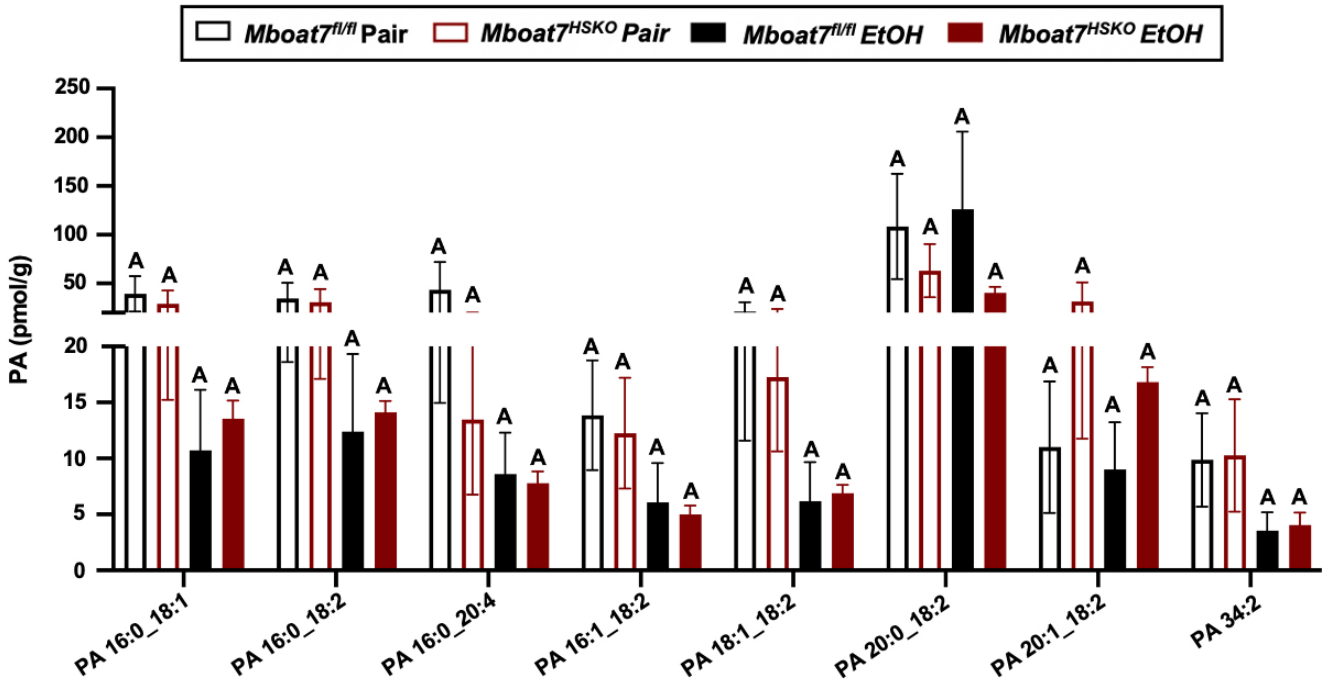

Figure 3 – Figure Supplement 9

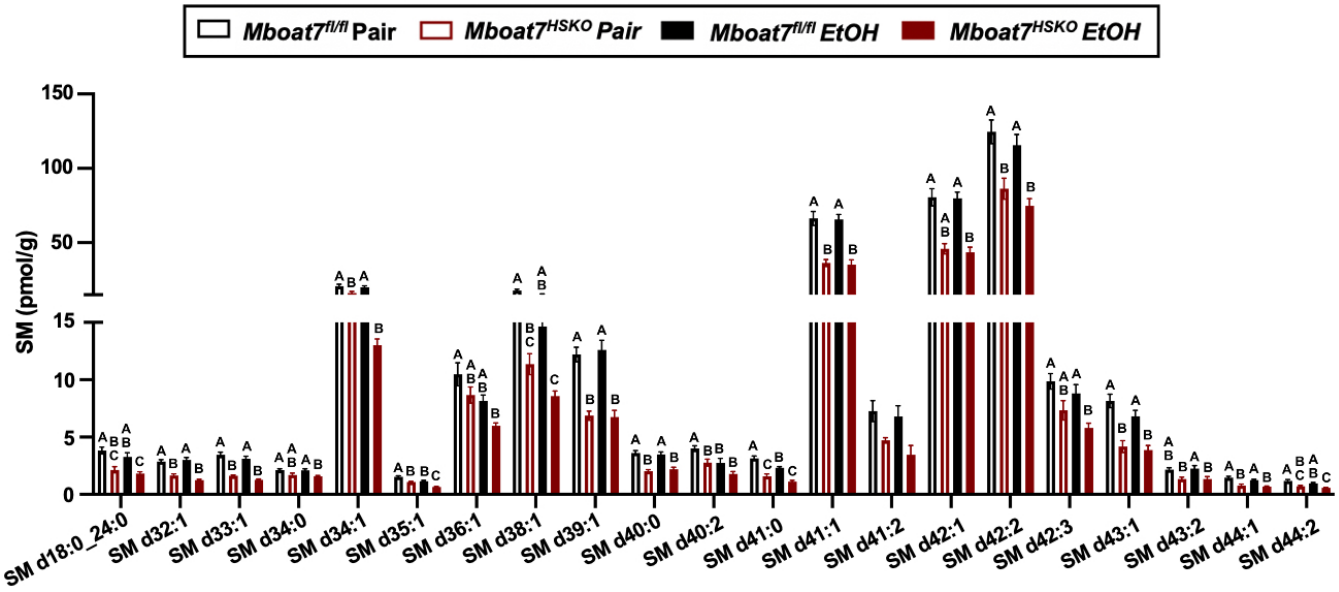

Figure 3 – Figure Supplement 10

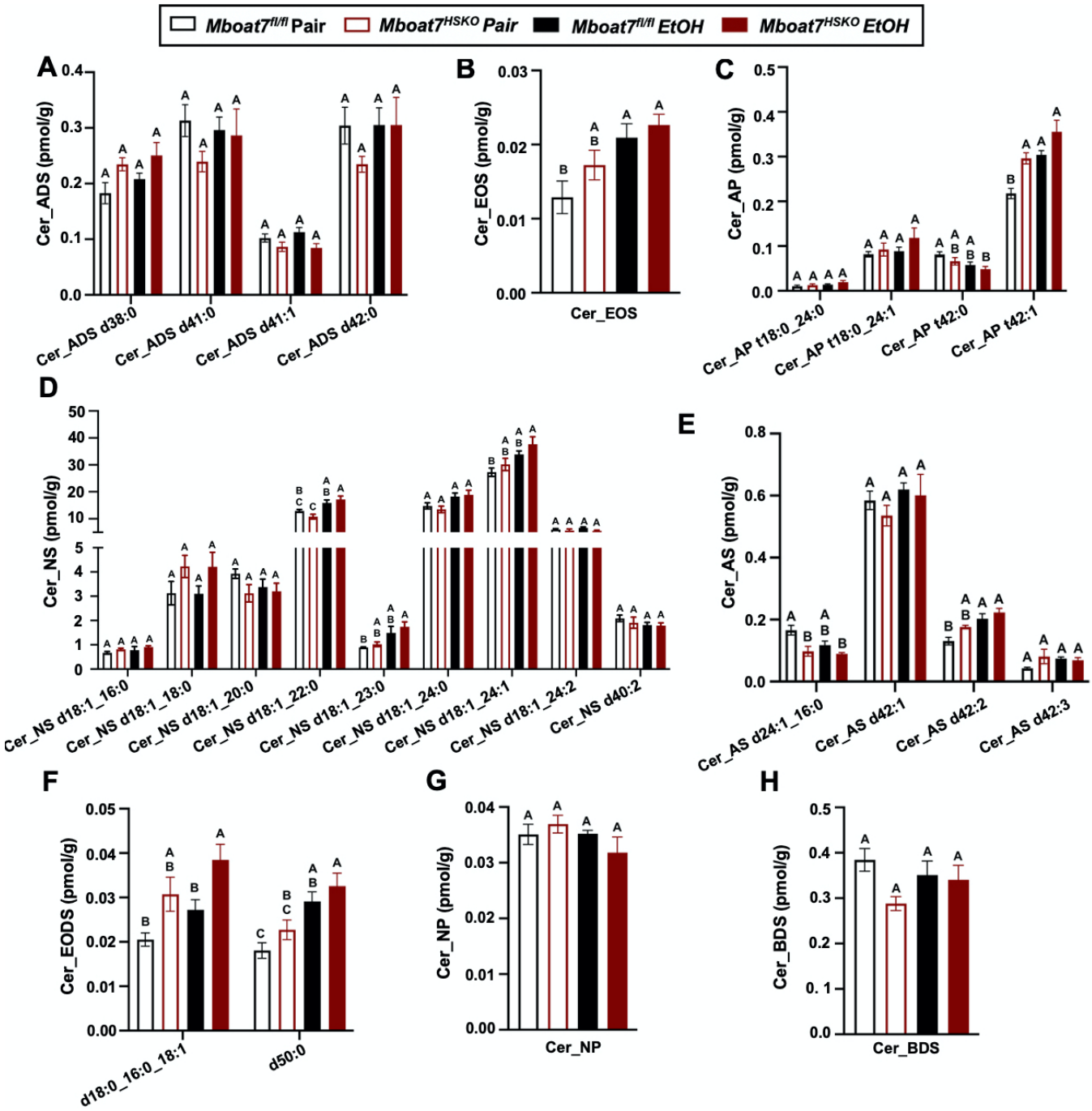

Figure 3 – Figure Supplement 11

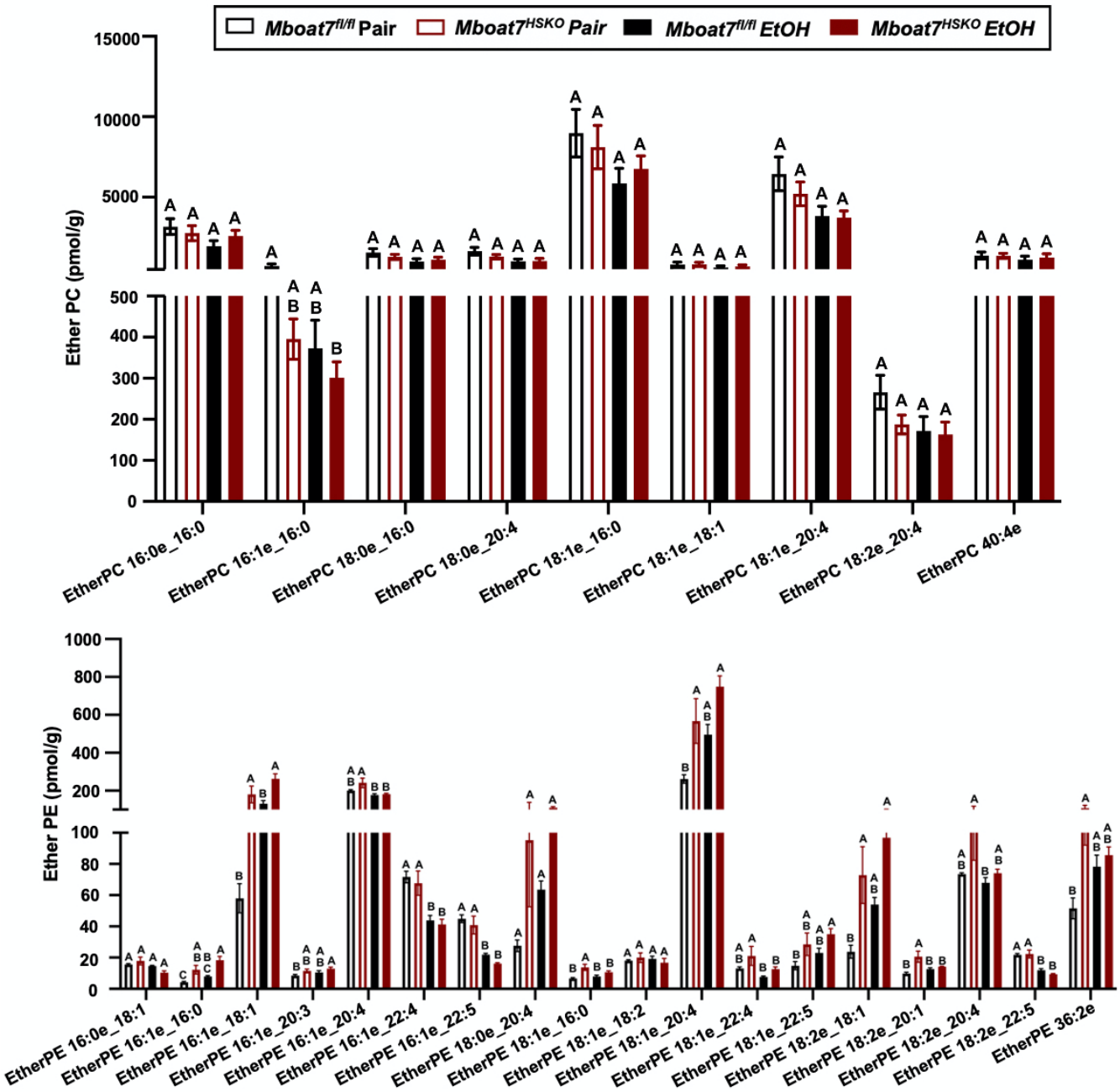

Figure 4

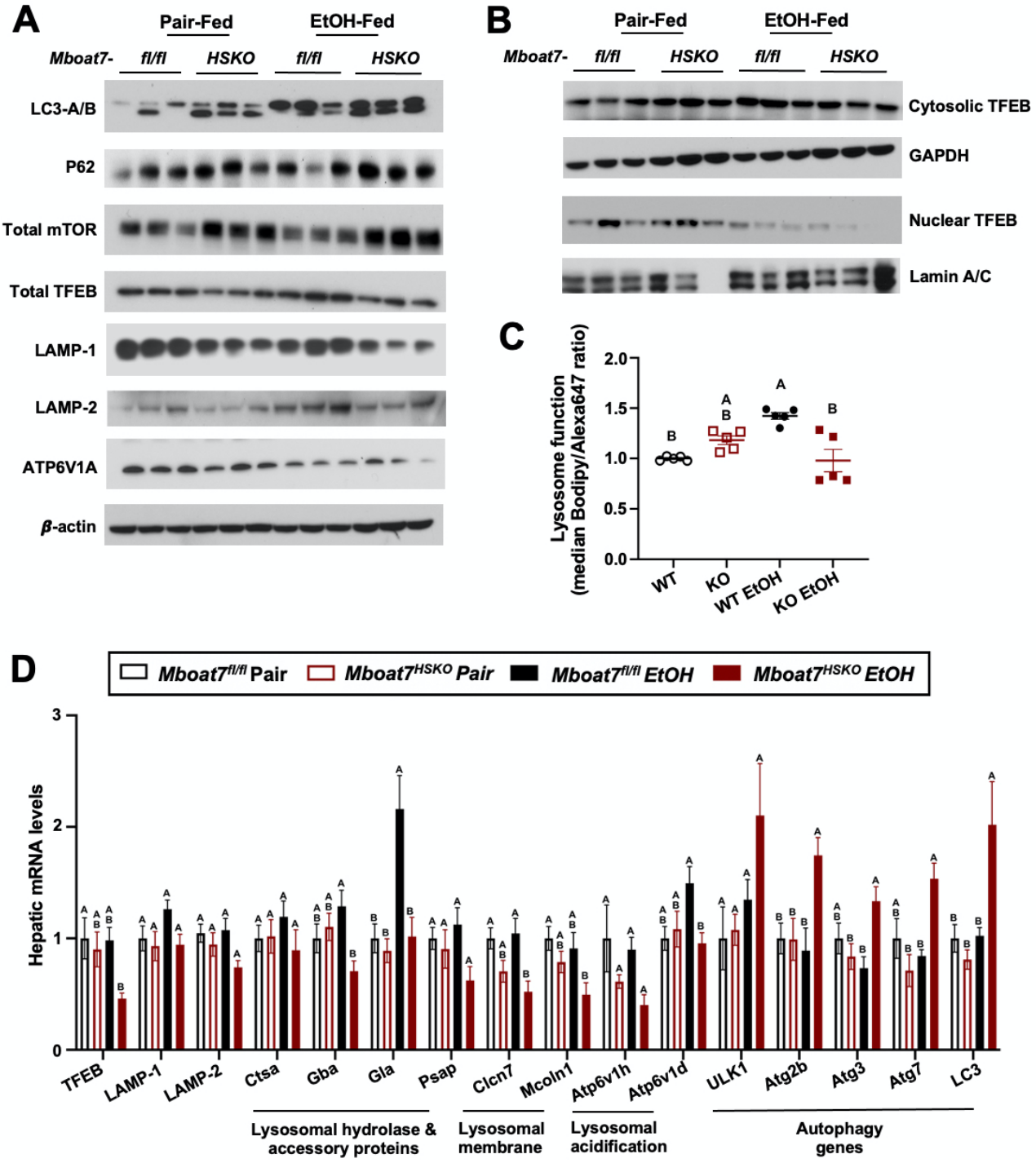
A
Pair-Fed
EtOH-Fed
Mboat7-
fl/fl
HSKO
fl/fl
HSKO
LC3-A/B
P62
Total mTOR
Total TFEB
LAMP-1
LAMP-2
ATP6V1A
β-actin
B
Pair-Fed
EtOH-Fed
Mboat7-
fl/fl
HSKO
fl/fl
HSKO
Cytosolic TFEB
GAPDH
Nuclear TFEB
Lamin A/C
C
Lysosome function
(median Bodipy/Alexa647 ratio)
2.0
1.5
1.0
0.5
0.0
WT
KO
WT EtOH
KO EtOH
D
Mboat7fl/fl Pair
Mboat7HSKO Pair
Mboat7fl/fl EtOH
Mboat7HSKO EtOH
Hepatic mRNA levels
3
2
1
0
TFEB
LAMP-1
LAMP-2
Ctsa
Gba
Gla
Psap
Clcn7
Mcoln1
Atp6v1h
Atp6v1d
ULK1
Atg2b
Atg3
Atg7
LC3
Lysosomal hydrolase & accessory proteins
Lysosomal membrane
Lysosomal acidification
Autophagy genes

Figure 4 – Figure Supplement 1

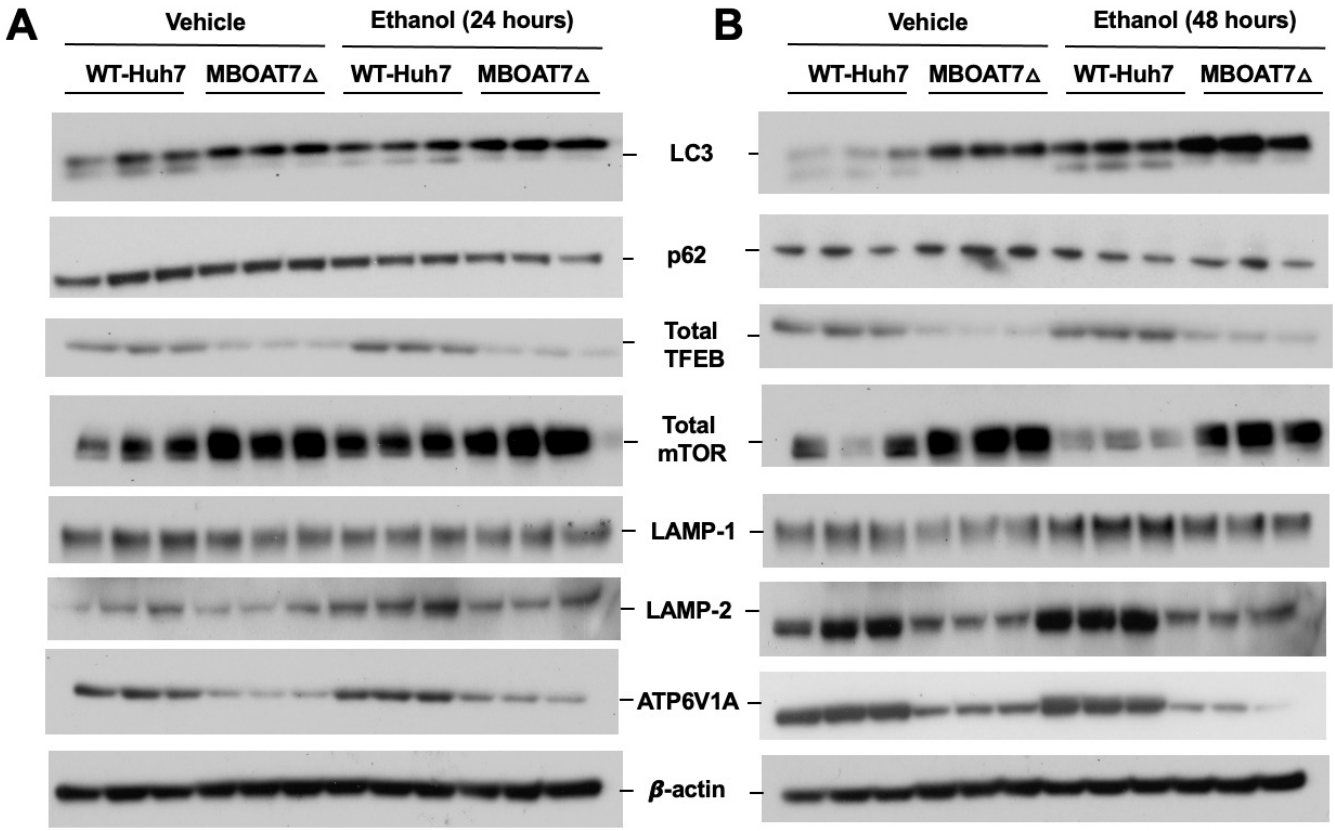
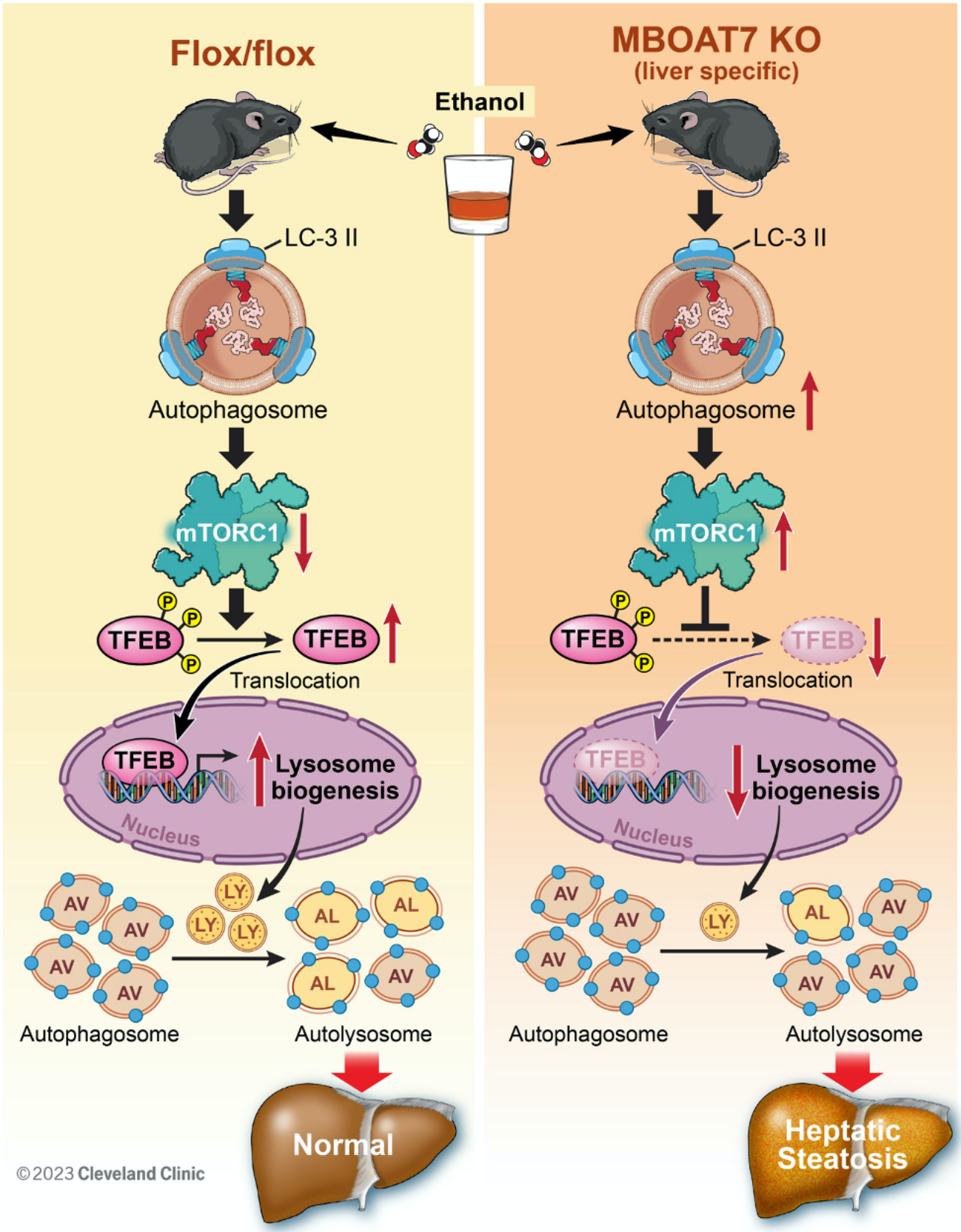
Figure 4 – Figure Supplement 2